UNIVERSITY OF CALIFORNIA
RIVERSIDE

# Ferromagnetic Resonance and Spin Hall Torque for Nanometric Thick Magnetic Insulator |Normal Metal Bilayers System

A Dissertation submitted in partial satisfaction
of the requirements for the degree of

Doctor of Philosophy

in

Materials Science and Engineering

by

Hamad Alyahyaei

August 2014

Dissertation Committee:

Dr. Jing Shi, Chairperson
Dr. Javier Garay
Dr. Nathaniel Gabor

The Dissertation of Hamad Alyahyaei is approved:

---

---

---

Committee Chairperson

University of California, Riverside

ABSTRACT OF THE DISSERTATION

Ferromagnetic Resonance and Spin Hall Torque for Nanometric Thick Magnetic Insulator |Normal Metal Bilayers System

by

Hamad Alyahyaei

Doctor of Philosophy, Graduate Program in Materials Science and Engineering
University of California, Riverside, August 2014
Dr. Jing Shi, Chairperson

In bilayer system, consists of ferromagnetic insulator, high spin orbit coupling normal metal (FM|NM), a new ferromagnetic resonance (FMR) damping that depends on varying the thickness of the normal metal observed. This new enhancement in the damping attributed to magnetic proximity effect (MPE) at the interface, which is verified by the increases in the real part of spin mixing conductance.

Spin pumping phenomena occurs when pure spin current can flow into the normal metal when the ferromagnetic film is at precession in bilayer system. The Onsager reciprocity implies that there must be a transfer of spin angular momentum from the normal metal to the magnetization of the magnetic layer. This effect is called; spin Hall torque ferromagnetic resonance (SHT-FMR). The combination of spin Hall effect and spin transfer torque allows the manipulations of spin wave damping and anti-damping by applying DC current at specific orientation to the DC field. In epitaxial nanometric thick yttrium iron garnet films (YIG) grown on gadolinium gallium garnet (GGG) substrates via pulsed laser deposition the SHT-FMR is extremely very low $J_s \sim 10^6 \frac{A}{m^2}$. This value can

not be explained by existence theory. The joule heating effect on the current induced SHT-FMR verified by temperature dependence FMR. The DC generated Oersted field evaluated by VSM. Power dependence on the FMR under varying the thickness might exhibit different critical thickness compare to the thickness where the enhancement of damping do saturate. Out of plane, FMR angular dependence was carried out to study extrinsic and intrinsic damping.

# Contents

# List of Figures

# Introduction

Spin-dependent phenomena have received massive interest from many research groups because of their technological potential. Almost two decades after the discovery of giant magnetoresistance (GMR)[8], extensive spintronics-related studies of metallic and semiconductor materials have confirmed that current disappears within a very short distance, mainly under the action of conduction electrons [9]. The development of a new route to overcome the limitations of electric circuits and to use pure spin current in spin-transfer torque devices is at the heart of the condensed-matter community's interest in developing technology beyond complementary metal oxide semiconductor technology. Most recently, a new emerging field called spin caloritronics[10] has addressed the generation of pure spin current using a temperature gradient. In his pioneering work, Slonczewski showed that a higher efficiency can be achieved in spin transfer torque using spin transport driven by the thermal gradient of a magnetic insulator/normal metal bilayer system[11].

The transmission of an electrical signal in a magnetic insulator was discovered in 2010[5]. Two types of carriers for non-equilibrium spin current can be identified: the conduction electron[12-14] and a collective motion of magnetic moments called a spin wave.[15-17]

In an insulator, the band gap prevents electron excitation[18] and a collective motion of spins can generate spin current that propagates for several centimeters[19].

Also in 2010, thermoelectric generation, which had been an exclusive feature of electric conductors, was demonstrated in a ferromagnetic insulator[20]. An electric voltage was generated by the heat flow in an insulator. This electric voltage is basically a spin voltage that can be detected via an attached normal metal that has strong spin–orbit coupling as a result of the inverse spin Hall effect.

These two breakthrough discoveries (i.e., the transmission of electrical signals by spin wave in a magnetic insulator and spin Seeback effect in magnetic insulators) have generated much of the research interest in the inter-conversion from spin current (i.e., the motion of spin angular momentum) to charge current and the transfer of spin angular momentum between the conduction electron of a normal metal and the magnetization of a ferromagnetic material. When a normal metal has strong spin–orbit coupling, the separation of oppositely spin-polarized electrons of charge current is called the spin Hall effect[21, 22]. The inverse process where the spin current is converted into charge current is called the inverse spin Hall effect[23, 24]. The inverse spin Hall effect allows the detection of the dynamic state of a ferromagnet[5, 25]. Moreover, the electron transport in the attached normal metal with strong spin–orbit coupling can be affected by static magnetization in the ferromagnetic material, and the separated electron spin owing to the spin Hall effect can undergo different spin-flip scattering on the interface with the ferromagnetic layer. This depends on the relative orientation between the magnetization and current direction, and has recently been called spin Hall magnetoresistance[26]. This completely new phenomenon was questionable, especially when it was investigated by X-ray magnetic circular dichroism (XMCD). The fundamental question is does the new magnetoresistance

originate from pure spin current owing to the transfer of angular momentum and the spin Hall effect at the interface, or is it just conventional anisotropic magnetoresistance?

The results of XMCD measurements have been controversial[27-29]. Some experiments have revealed an induced magnetic moment on normal metals, whereas others showed no evidence of such a moment at the interface. These inconsistent results might be explained by the mechanism used to estimate the moment induced on the normal metal, and ensuring the quality of the yttrium iron garnet (YIG) surface at the interface is paramount. The proximity effect is a completely surface-related phenomenon; the better engineered the surface, the more clearly the intrinsic phenomena manifest.

First-principles calculations employing density functional theory were performed for a YIG|normal metal system. The normal metal was Ag[30] in one study and Pt and Au in another[27]. Density functional theory revealed that a pronounced magnetic moment is induced on all normal metals except Au. A more detailed calculation took into account the cutting of the surface with termination at an iron, oxygen or yttrium atom and concluded that, for all termination possibilities, the proximity effect generates a moment on the normal metal[30].

At the interface between ferromagnetic (FM)|(NM); The dynamical magnetization pumps a pure spin currents into the adjacent normal metal. The efficiency of this process –spin pumping- are governed by a constant called spin mixing conductance. This constant is given by

$$G_{\uparrow\downarrow} = \frac{1}{2}\sum_m(|r_{\uparrow,m} - r_{\downarrow,m}|^2 + |t_{\uparrow,m} - t_{\downarrow,m}|^2),$$

where $r_{\uparrow(\downarrow),m}$ and $t_{\uparrow(\downarrow),m}$ are the reflectivity and transmission parameters for the spin majority (minority) of the normal metal at the channel $m$ on the interface between (FM)|(NM).

More important is the ability to distinguish between metallic and insulating ferromagnetic film attached to a normal metal in terms of the role of spin mixing conductance constant $G_{\uparrow\downarrow}$. In both systems, spin-mixing conductance affects the possibility of generating a pure spin current[30, 31]. This constant contains two terms that define the spin majority (minority) reflectivity and the transmission parameter. In a metallic system, this constant is distinct; experimental and theoretical predictions are in good agreement[31, 32]. In magnetic insulators, the transmission parameter is zero[30], however, the reflectivity parameter includes a phase that depends on the channel number, thus resulting in a non-zero value for the mixing conductance constant at the interface between the magnetic insulator and normal metal[30].

In interpreting the transport measurement results, three basic constants should be taken into account: the spin diffusion length, the spin Hall angle, and the spin-mixing conductance. Sets of these parameters can be obtained by fitting to a set of data for each transport experiment. However, one if not two constants is typically set to what is commonly used or has been reported in the literature. This estimation might lead to misinterpretation of the transport results for the magnetic insulator/normal metal system.

A ferromagnetic resonance (FMR) experiment can easily overcome this problem and identify at least one if not all the fundamental constants without the need to estimate or use previous knowledge of one of the constants. This was demonstrated recently in 2014 by combining FMR, spin pumping, and inverse spin Hall effect experiments on Co/Pt bilayers and Co/Cu/Pt trilayers. The results clearly showed spin memory loss governed by surface perfection in the metallic systems[33].

The enhancement of the Gilbert damping in thin film has been well demonstrated for metallic ferromagnetic films[31, 32, 34-36] and recently for insulators[4, 5, 37-41]. This damping is realized through i) the energy distribution within the magnetic subsystem, ii) the energy transfer from the magnetic subsystem to a nonmagnetic subsystem such as a phonon and iii) spin pumping when the magnetic film is in contact with a normal metal. The first two types of damping mechanisms are all within the ferromagnetic system and the third transfers energy into an external system of a normal metal attached to the ferromagnetic film. The behavior of this damping can be used in studying several fundamental phenomena and to investigate the existence of ferromagnetic order owing to the proximity effect.

Attaching a normal metal to a ferromagnetic film leads to further enhancement of the Gilbert damping. Such enhancement behaves in different ways depending on whether a metal with strong spin–orbit coupling is placed in direct exchange or non-direct exchange with the ferromagnetic film. Direct exchange results in a linear increase in the damping constant before it reaches saturation, which is the limit of spin pumping. Non-direct exchange enhances the damping in an exponential fashion. This latter exchange occurs when the metal with strong spin–orbit coupling is separated from the ferromagnetic film by a metal with weak spin–orbit coupling. An XMCD experiment showed that, in samples with linearly enhanced damping, a moment is induced on the normal metal. Moreover, in samples with exponentially enhanced damping, no moment is induced owing to the presence of the spacer with weak spin–orbit coupling. This indicates that FMR can be used as a completely new route to identify the existence of a moment induced by the proximity effect[42].

First-principles calculation has shown that placing a ferromagnetic metal between YIG ferromagnetic insulator and Ag normal metal increases the spin-mixing conductance constant by 40–60%[30]. This can be used as a further judging criterion for confirming the magnetization of the first few layers of the normal metal when placed in contact with ferromagnetic insulator film. This enhancement has been confirmed experimentally[6].

The Onsager reciprocal relation implies that, if the resonance of a YIG film generates a voltage via the inverse spin Hall effect, then there must be a transfer of angular momentum from the normal metal with strong spin–orbit coupling to the magnetization of the YIG insulator. This means that one could manipulate the relaxation of the

ferromagnetic film by applying a direct current to the adjacent metal. This effect has been demonstrated for micrometer-thick YIG film[3, 5], and a damping and anti-damping modulation took place when applying a positive and negative current in a specific orientation. This effect has been well established for a nanometric metallic bilayer system[43-46]. In a metallic system, high current density of $10^{10}$ A/m$^2$ is required to establish spin Hall torque[43]. For micrometer-thick YIG film, this phenomenon exhibited a strongly non-linear behavior, but most importantly, the spin Hall torque was induced at extremely low current density of $10^8$ A/m$^2$.[5] This value has not been explained by any theoretical model. Additionally, very few works have investigated this system to justify or reproduce the results, and all such work has been on micrometer-thick YIG film[47, 48]. Different groups have reported spin Hall torque starting at current densities ranging from $10^8$ to $10^{10}$ A/m$^2$.[3, 5] Even though a current density of $10^8$ A/m$^2$ is considered to be very low since it does not agree with the theoretically predicted value estimated for the bulk excitation that corresponds to the macrospin mode as[49]

$$J_c = \left(\frac{1}{\theta_H}\right)\frac{e\alpha\omega M_s t}{\gamma h} \sim 10^{11\sim12}\,\frac{A}{m^2},$$

Where $e$ is the charge of electron, $\gamma$ is the gyromagnetic ratio, $\omega$ ferromagnetic resonance frequency,$\theta_H$ is the normal metal spin Hall angle, $t$ is the ferromagnetic layer thickness, $\alpha$ and $M_s$magnetic damping and saturation magnetization respectively.

This current density is far from being implemented into STT technology. The first attempt to verify the spin Hall torque in nanometric YIG film was carried out on 200-nm liquid phase epitaxy (LPE) film[50]; however, the phenomenon was not observed even at low

temperature and high current density of $10^9$ A/m$^2$. Spin Hall torque expected to occur for the line-width of the YIG film.

Recently, in April 2014[51], a theoretical proposal concluded that spin torque FMR should provide valuable information on the current-induced magnetization dynamics of insulating magnets and has very promising technological implications for very-low-power data transmission. However, most relevant to the phenomenon is that reducing the thickness of the film should reduce the current density. Additionally, future investigations will sandwich ferromagnetic insulator film between two normal metal films one with strong spin–orbit coupling to induce the STT-FMR effect, the second metallic layer having weak spin–orbit coupling to eliminate any heating effect.

For our YIG film grown via pulsed laser deposition (PLD) and having thickness ranging 10–30 nm, we investigated the effect of direct current and observed an STT-FMR effect at extremely low current density; i.e., down to $10^5$ A/m$^2$ in one sample and even lower density of $10^3$ A/m$^2$ in another sample. These extremely low densities are reproducible, and a more extensive effort is needed to better understand the mechanism behind the spin transfer torque effect at low current density in nanometric YIG film.

An other phenomenon to be taken into account for this system is the power dependence of the spin pumping effect in YIG film. Many systematic measurements have been made by several groups on the power dependence and related non-linear phenomena in thick YIG film[52]. More recently, the relation between the power and thickness of YIG has been taken into account, for YIG thickness ranging from 20 to 300 nm. The two-

magnon scattering process at the interface is more pronounced for thinner films and gives rise to additional damping. After confirming the induced magnetic moment on the metal attached to YIG film, we have investigated the possibility of inducing greater damping from two-magnon scattering at the metal surface in addition to the YIG surface, which would lead to further enhancement of damping that could not be observed at low power.

The insulating material responsible for generating this interest is YIG. The large distance of spin wave propagation is owed to the very weak magnetic damping. The damping in YIG is the weakest in ferromagnetic material at room temperature[53]. Additionally, YIG has other attractive properties, such as a high Curie temperature, good insulation, high chemical stability, and easy synthesis with different routes and methods. YIG has been used in optical, microwave, and data storage technologies[53].

Because of its very small Gilbert damping coefficient ($2 \times 10^{-5}$), YIG is considered the best medium for spin wave propagation. Electron-mediated angular momentum transfer can only occur at the interface between YIG and a metallic layer. The metallic layer should have strong spin–orbit coupling; e.g., Pt, Pd, Ta, W or CuBi. This choice of metal ensures the generation of pure spin current via the spin Hall effect. The interface is governed by the so-called spin-mixing conductance constant $G_{\uparrow\downarrow}$

The amount of angular momentum transformed from YIG is scaled inversely with the YIG film thickness ($1/t$; where $t$ is the YIG thickness)[49]. It is important to reduce the YIG thickness to nanometric scale and maintain the magnetic properties of the material, especially the weak Gilbert damping and saturation magnetization.

The first attempt to grow nanometric YIG employed liquid phase epitaxy (LPE) and realized ultimate thickness of 200 nm[54, 55]. To reduce the thickness beyond what is possible employing LPE, another growth method should be used, such as PLD, which is a versatile technique for growing an epitaxial oxide film.

Many groups are investing massive effort into growing an ultra-thin YIG film via PLD. Very high quality films have been obtained. However, the most important factor besides the damping constant is the spin-mixing conductance constant which means after introducing a metal to be in contact with the YIG film.

## Ferromagnetic Resonance

Griffiths designed the first ferromagnetic resonance experiment, and Kittel developed the initial theory. FMR is one of the most powerful tools for studying the magnetic properties of nanometric films. An FMR measurement can extract substantial information about the magnetic sample, such as the magnetic anisotropy, magnetic moment, magnetoelectric coupling constant, Curie temperature, damping constant, and relaxation mechanism of the magnetization. More recently, FMR measurements have revealed more information about the spin wave excitation, spin current generation, the estimated spin Hall angle, the spin diffusion length, electron–magnon interaction and magnon–magnon interactions.

In magnetic materials, the total moment precesses at the Larmor frequency around the local static magnetic field. The spin resonance in ferromagnetic materials occurs when the energy of small transverse microwave field rf-field is absorbed when the rf- frequency overlaps with the precession frequency.

The motion of the magnetization is described by the Landau-Lifshitz-Gilbert equation of motion,

$$\frac{dM}{dt} = -\gamma[M \times H_{eff}] + \frac{\alpha}{M_s}(\vec{M} \times \frac{d\vec{M}}{dt})$$

The first part of this equation corresponds to the precession and the second part introduce the Gilbert damping constant $\alpha$, $H_{eff}$ do include the applied DC magnetic field and the rf-field as well, $\gamma$ is the gyromagnetic ratio given by

$$\gamma = \frac{g\mu_B}{\hbar}$$

where $g$ is the spectroscopic splitting factor, which is measured for electron to be 2.0, $\mu_B$Bohr magneton constant given by $\mu_B = \frac{e\hbar}{2m_e c}$ this process can be simply sketched as in figure 1.

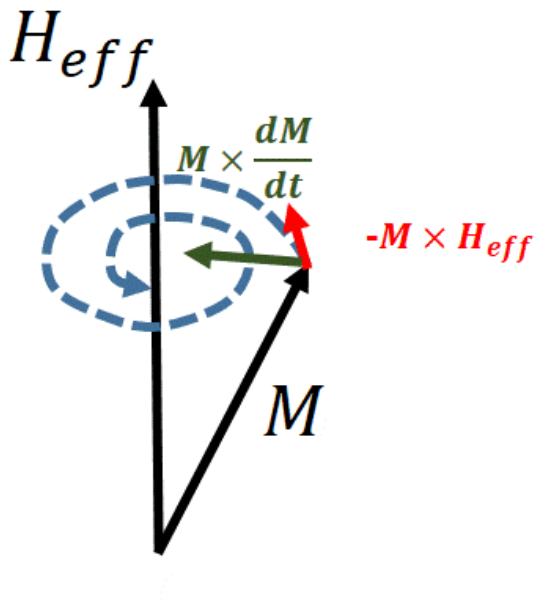


Figure 1: Landau-Lifshitz-Gilbert equation simplified graphical representation under the assumption that $H_{eff}$ is constant; Precession (red) and damping (green) and the trajectory of the magnetization is dashed blue curve.

At the microscopic level, the DC field causes a Zeeman splitting in the energy levels, the transition of magnetic dipole between the energy levels would happen under varying the DC magnetic field. Figure 2 is a graphical representation for Electron Spin Resonance (ESR). The Zeeman splitting and the magnetic dipole transition where the resonance spectrum occurs. Nevertheless, in FMR we have a large number of electron spins exchange locked together and precess in an effective magnetic field.

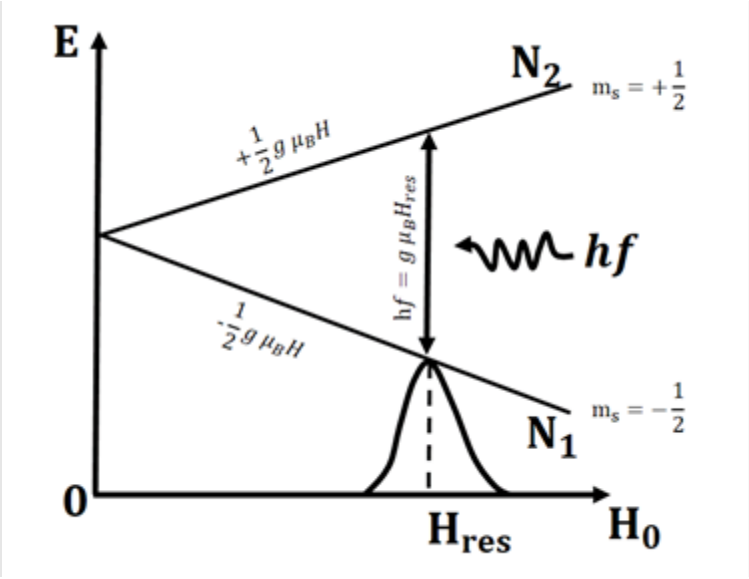


Figure 2: Diagram of the Zeeman splitting and the magnetic dipole transition diagram. The transition occurs under a fixed microwave frequency and a varying DC magnetic field. This is for single spin

In most FMR conventional spectroscopy systems, the absorption derivative is collected because FMR signals represents a very small variation in the overall absorption of microwave power in a cavity. The small variation forces us to amplify the signal. Then it is done by adding a small oscillating magnetic field to the large external field. This process is called modulation of the magnetic field. For samples with a very narrow line-width, it's very important to keep the modulation amplitude much smaller than the

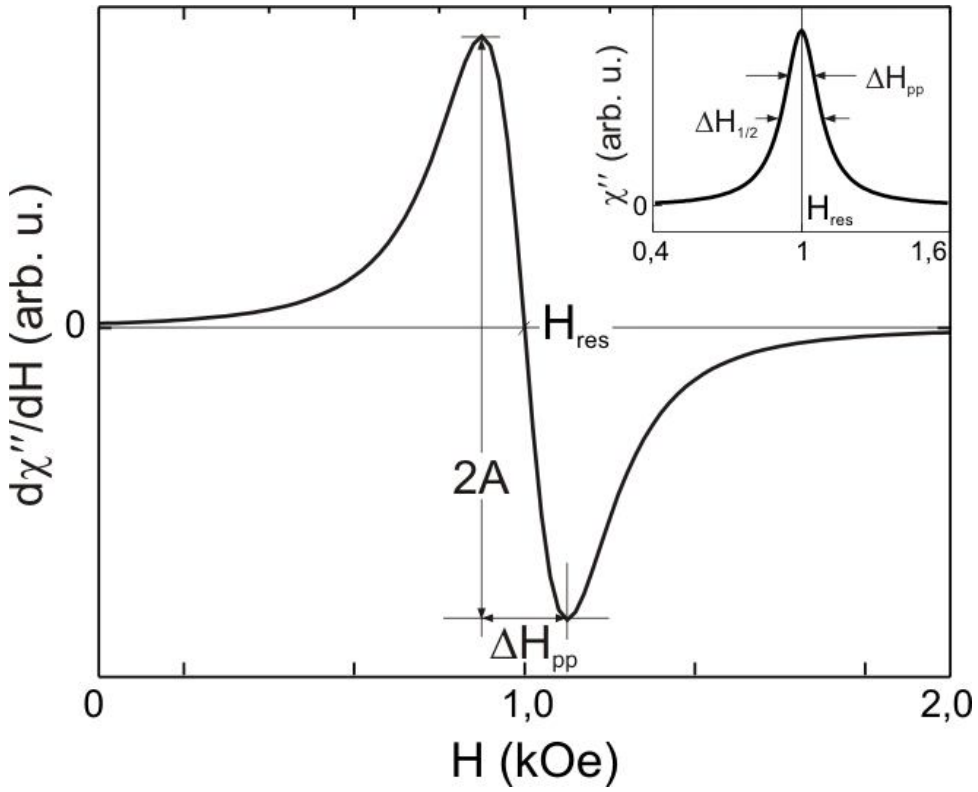


Figure 3: Schematic representation of the FMR responses of a ferromagnetic film at fixed frequency $\omega$. The inset shows the dissipative susceptibility tensor $\chi''$.

minimum line-width of the FMR spectrum. In our setup, we have a minimum modulation of 0.01 Oe which is about 300 times less than the minimum observed line-width of nanometric thick yttrium iron garnet (YIG) films. The resonance spectrum line shape looks like a Lorentzian as shown in Figure 3. The resonance filed position depends on several factors the most important one is the angle of applied filed and the magnetization of the sample. The line-width ΔH represents the relaxation processes in the magnetic material. In nanometric thin films, the line-width represent the uniformity of the film, Gilbert damping

and several other relaxation processes such as spin pumping, and magnon-magnon scattering.

The angular dependence the resonance field can provide information about the saturation magnetization under certain circumstances A, simplified way to obtain the saturation magnetization without performing an extensive fitting for the angular dependent FMR spectrum is to apply the DC field in-plane or out of plane. In this work most spectra are collected with in-plane fields, where the saturation can be obtained from the equation below.

$$\frac{\omega}{\gamma} = \sqrt{H_{res}(H_{res} + 4\pi M_s)}$$

## Yttrium Iron Garnet (YIG)

YIG is a ferrite that exhibits a very low coercive field and has been implemented in several technological applications. The unit cell contains a 160 atoms with two sites for the iron atoms at the octahedral and tetrahedral sites, with a lattice constant about 12.38 Å. Our nanometric thin films are deposited via pulsed laser deposition (PLD) in an ozone environment under well-controlled deposition condition that is reported by Tao Lin et, all[56], and initial search for the recipe is reported within Tao thesis[57]. The pulsed laser deposition is a versatile technique for growing epitaxial thin films, especially films of oxide materials. A basic description of our laboratory PLD system was reported the thesis of Liu, who worked under the supervision of Professor Jing Shi at UC Riverside.[58] To summarize the

basic elements of the growth, we stress the fact that our YIG films exhibited a perfect single crystal surface crystallography, which was verified by the sharp and high Laue zone order

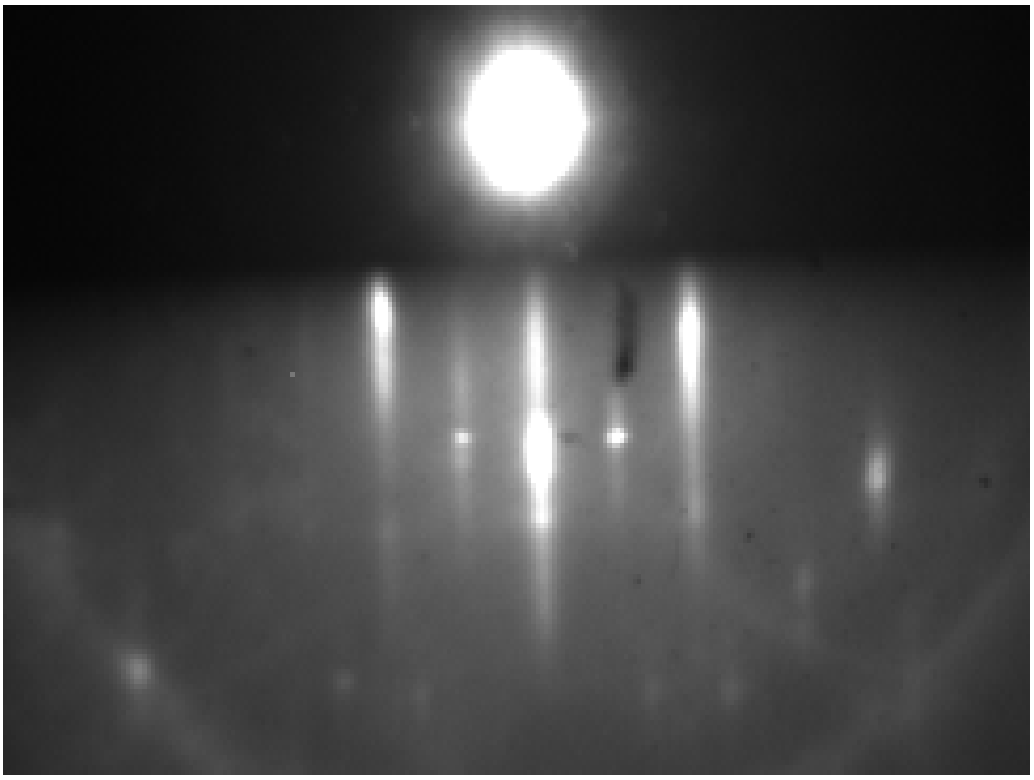

Figure 4: The sharp and high intensity streaked RHEED pattern from the YIG (110) surface indicates that the sample had a terraced surface. Credit to Tao Line.

determined from the reflection high energy electron diffraction (RHEED) pattern shown in figure 4.

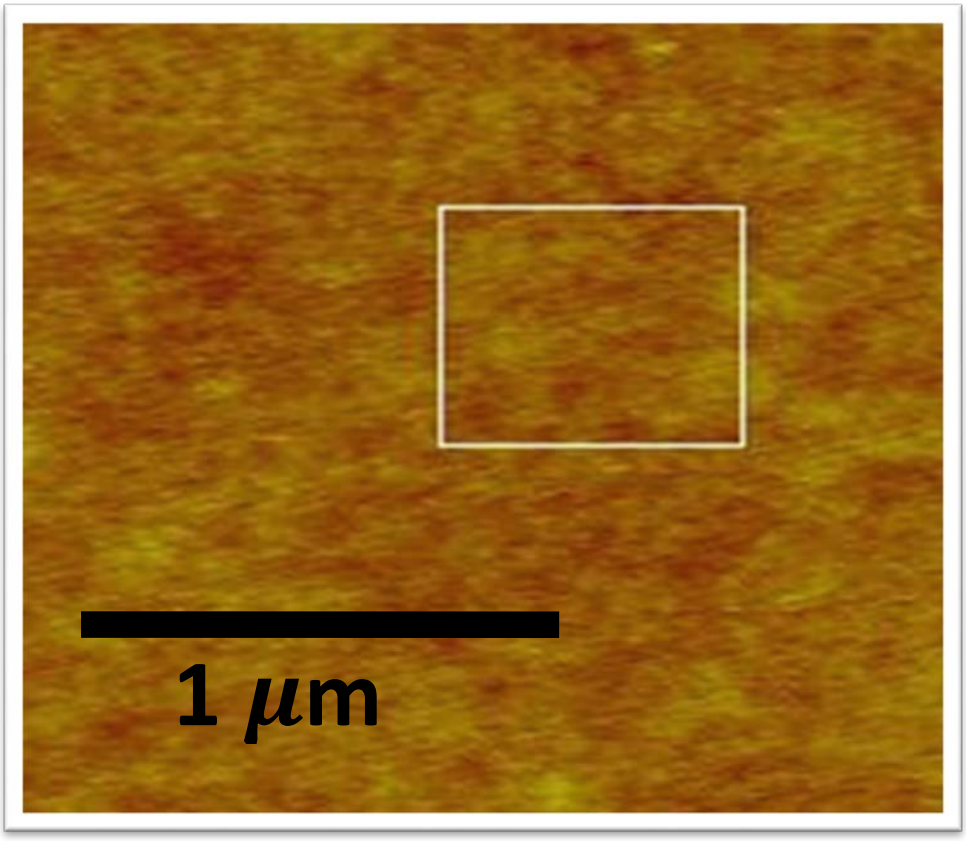


Figure 5: AFM image of the YIG (111) average mean roughness (RMS) of 0.08 nm.

It is very important to have a surface with single crystal phase. The sharp and intense RHEED line can be used as an indicator of the flatness of the surface which is verified through Atomic Force microscope (AFM) Figure 5. Our film surface mean roughness falls between (0.06-0.08)nm. This mean roughness is below what has been reported in 2012 which ranges between (0.1-0.3)nm[59], more recently in 2013 with a mean roughness of 0.23nm$^2$.

The thickness can in principle be controlled by counting the RHEED oscillations if the entire growth has RHEED oscillations. Growing such an atomically flat thin film is very crucial to the understanding of the interface between ferromagnetic insulator and normal metal or any different material. It has been verified by cross-sectional transmission electron microscope (TEM)[1] shown in Figure 6 in which a flat YIG surface shows a well-controlled Pt|YIG interface. The second image shows a sub-nanometer-scale amorphous

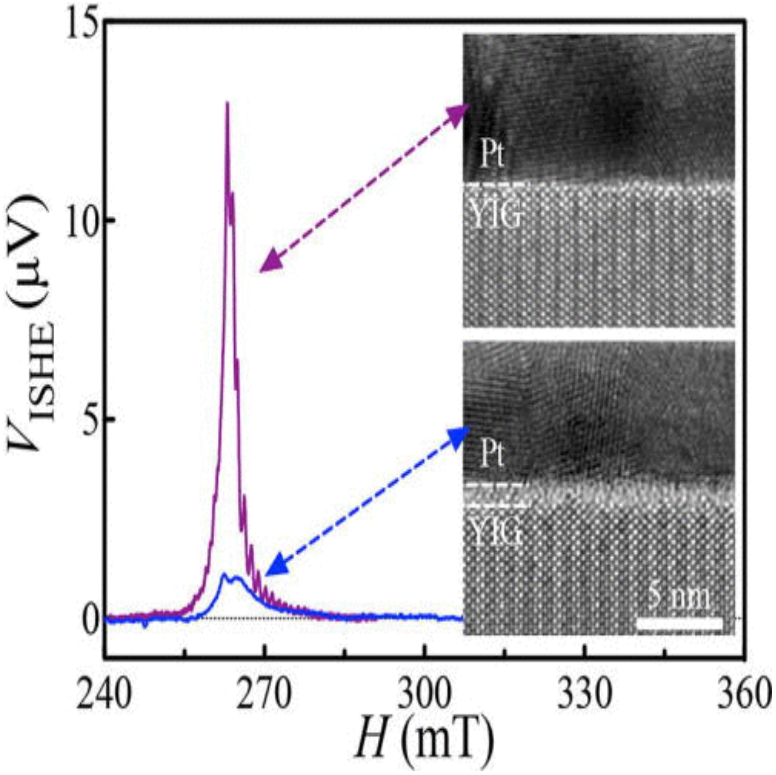


Figure 6: cross-sectional TEM image of well-controlled interface and intentionally roughed surface to observed interface effect on ISHV. Figure from [1, 2]

layer at the interface between Pt|YIG. We can see from the figure 6 how flatness plays a very important role in magnifying the transparency of transferred angular momentum from ferromagnetic film to a normal metal film. This at least has an effect of one order of magnitudes on the measured inverse spin Hall signal (ISHE) which we will discuss later. One more very important point to keep in mind is the spin mixing conductance constant $G_{\uparrow\downarrow}$even at a perfect interface between Pt|YIG[1] in figure has reported a value for $G_{\uparrow\downarrow}$less by an order of magnitude compare to the theoretically predicted value. The theoretical predicted value based on the first principles calculation has been carried out for Ag|YIG system, where Ag has a lower spin-orbit coupling compared to Pt, then in Pt $G_{\uparrow\downarrow}$is supposed to be higher than that of Ag. The theoretical value for the real part of $G_{\uparrow\downarrow}$ $\sim 10^{14}(\Omega^{-1}\mathrm{m}^{-2})$. For micrometer thick films with good interface, the maximum reported value is $\sim 5 \times 10^{13}(\Omega^{-1}m^{-2})$. This will bring us back to the need of scaling down to nanometric thin YIG films based on the prediction that the transparency of the angular moment is scaled inversely with the thickness of the ferromagnetic film. Another important point is flatness at the level of sub-nanometer level can only be achieved by epitaxial growth technique. This roughness at the atomic level will offer a platform to grow the normal metal with thickness below the spin diffusion length, which is in most cases for high spin-orbit normal metals below 2nm at room temperature.

## FMR measurement on Nanometric thick YIG

For the first set of measurements the FMR data for in-plane or out of plane for PLD-YIG was complex were the extra peaks can't be understood or interpreted as spin wave, as in figure 7:

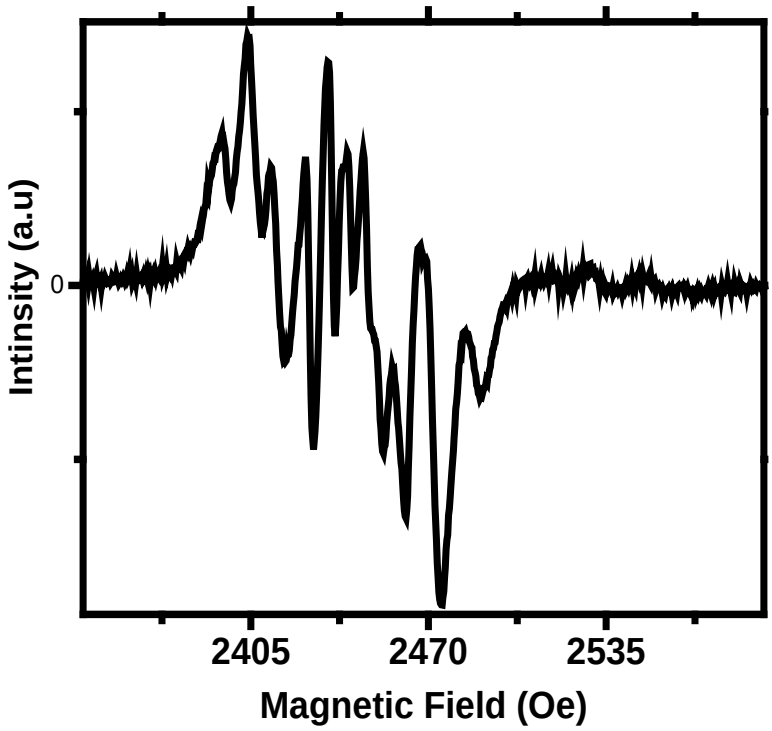


Figure 7: FMR spectrum for thin YIG film, the extra peaks cannot be assigned to any spin wave mode.

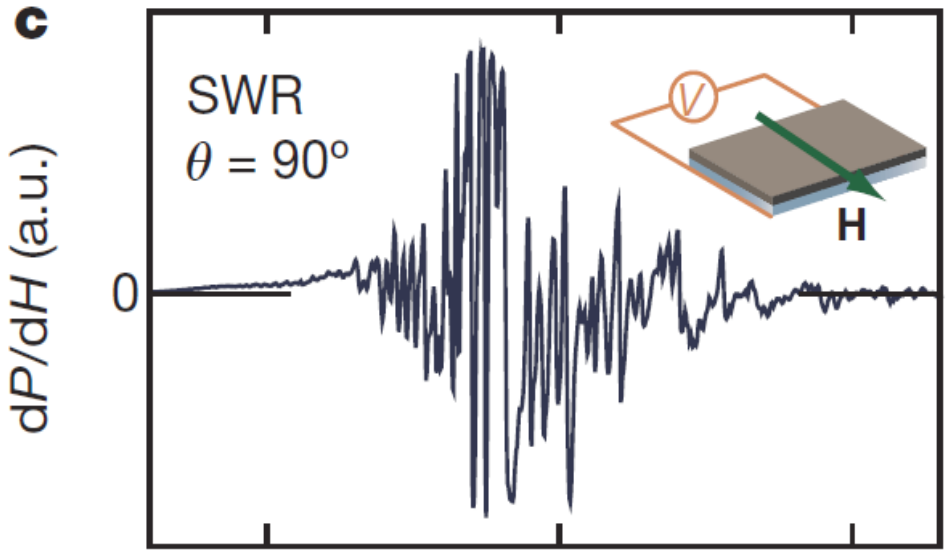


Figure 8: FMR spectrum of micro-meter thick YIG film grown by LPE, as reported in the poineering work in the field of trensmiton of electrical signal in insulator [5]

Even though the first work on the transmission of electrical signal in insulator[5] has reported a very closely spaced FMR signal figure 8, this fine structure has been interpreted to be caused the size quantization of spin wave due to the finite lateral extension of the sample[49]. The physics of this fine spacing and the quantization of spin wave has not been explored yet. From experimental point of view such a signal can only be interpreted to be due to non-uniformity of the film. This is because non of the signal can be fitted with spin wave models. This has been investigated in a Ni-Mo superlattice FMR study[60]. Carrying detailed angular dependent FMR can help analyze the effect of the sample non-uniformity in magnetization. The rotation requires a precise sample rotator to avoid modifying many intrinsic parameter such as saturation magnetization or sample size to fit spin waves models like Damon Eshbach mode DEM, magnetostatic volume forward and backward mode MSVFM and MSVBM respectively.

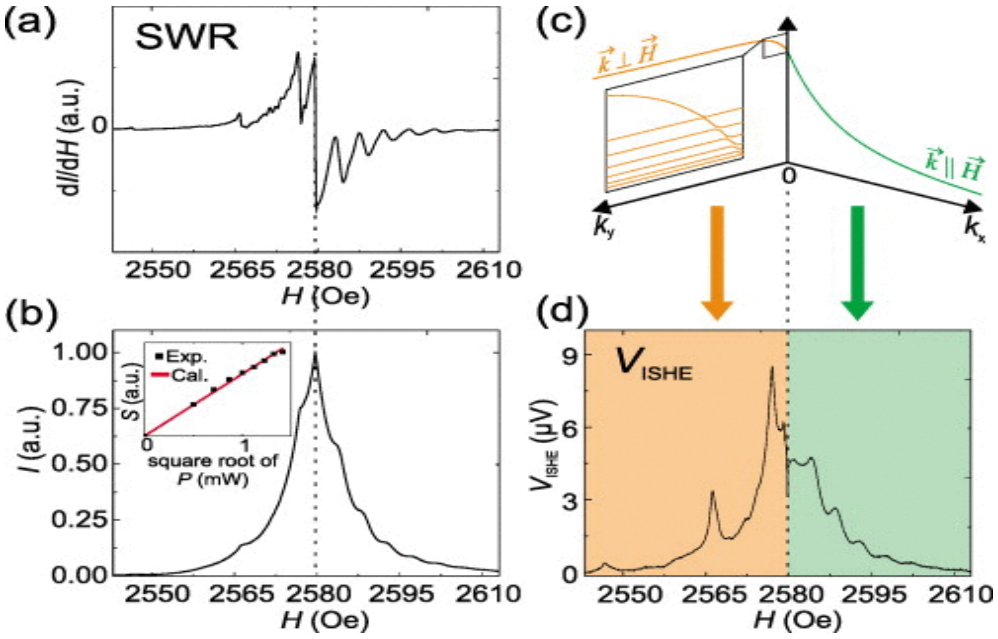


Figure 9: FMR in b and ISHV in d the main peak does not necessarily represent the uniform mode k=0. [4]

Identifying the main FMR peak in a sample that exhibit many and tiny spaced FMR peaks is possible by integrating the FMR spectrum and to pick the peak with the highest intensity. This method has been adopted very well within the FMR community. Recently a work on the enhancement of spin pumping efficiency by spin wave mode selection[4] showed that surface mode can have highest intensity. If the main peaks always represent the highest intense signal then this should be the case for all the measurement tool, spin pumping via coplanar wave guide or cavity and more importantly is the collection of the signal via energy absorption or invers spin hall voltage. Figure 9 shows the change in the

location of the highest intense peaks under changing the tool of identifying the spin wave mode in Pt|YIG system.

Very few groups have carried out the PLD growth of nanometric thin YIG films. Most previous studies before[61] 2010 focused on a thickness range close to or at the LPE limit which is $0.2\mu m$ with comparable quality to YIG single crystal in term of the line-width $\Delta H$ and saturation magnetization $4\pi M_s$. To be at the thickness of less than 50nm is a challenging task if the demand is to mimic the thick film magnetic properties specially the damping and uniformity, because at thinner film enhancement of Gilbert damping will appear due to several reasons.

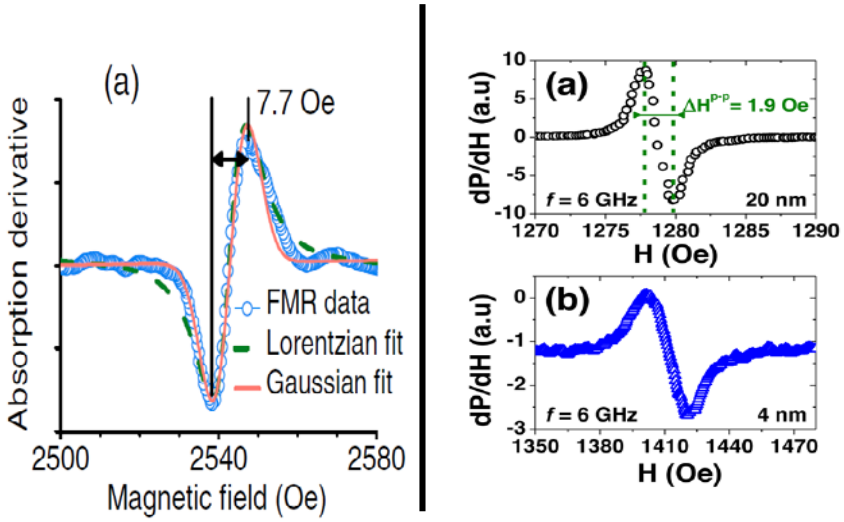


Figure 10: Single peak PLD nanometric thick YIG film has been reported by several groups. The Lorentzian shape cannot be fitted as a single peak[6]. The thinnest YIG film is 4nm.[2]

The magnetization uniformity can be judged from the shape of the resonance features and quantitatively from the Lorantzian fitting of the FMR spectrum. When single Lorntzian is resulted from the fitting of the experimentally obtained FMR spectrum then the film can be described by a uniform magnetization. It has been pointed out recently 2013[6] that the Gaussian function fits the data better than the Lorentzian function. Figure 10 shows different groups FMR spectrum which confirm this find[2].

## Annealing effects on FMR

We start investigating the growth condition and annealing effect on the FMR signals. The growth conditions or parameters are modified in terms of growth temperature and ozone pressure. The leaser pulse energy and frequency were kept fixed for all samples. The annealing was carried out in another chamber in oxygen environment at high temperature ~ 850 $C^o$.

Annealing the samples out of the PLD chamber has shown an increase in magnetization measured by vibrating sample magnetometer (VSM) measurement[57], but FMR is sensitive to subtle property changes and can provide more detailed information. For example, to obtain the saturation magnetization of YIG from VSM data we should first exclude the paramagnetic background from the substrates, also need precise information about the volume of the magnetic film. It's always possible to do both the subtraction of the paramagnetic signal and the volume but this always takes some estimation into account. FMR, on the other hand, provides more reliable information about the saturation magnetization $4\pi M_S$. But at the nano-metric thickness level, the saturation magnetization differs from the tabulated value of YIG $4\pi M_s \sim 1700$ Oe. This is due to the off stoichiometry[61] effect which has been report in PLD grown YIG films. Then we focus our attention to one single parameter which is the line-width. Bulk YIG is well known for its unique line-width to be the smallest among all the ferromagnetic materials. From the annealing process we want to find out if the annealing in oxygen or ozone environment

would obtain narrower line-width compared to the initial value for YIG film without annealing. The annealing process has be carried out three times on each sample for 6 hours at 850 C$^{o}$. figure 11 shows the FMR results of one out of more than 15 sample to confirm the annealing effect.

The conclusion is that any further annealing for the YIG thin film will not improve the quality of the sample. Without performing X-ray photoelectron spectroscopy (XPS),

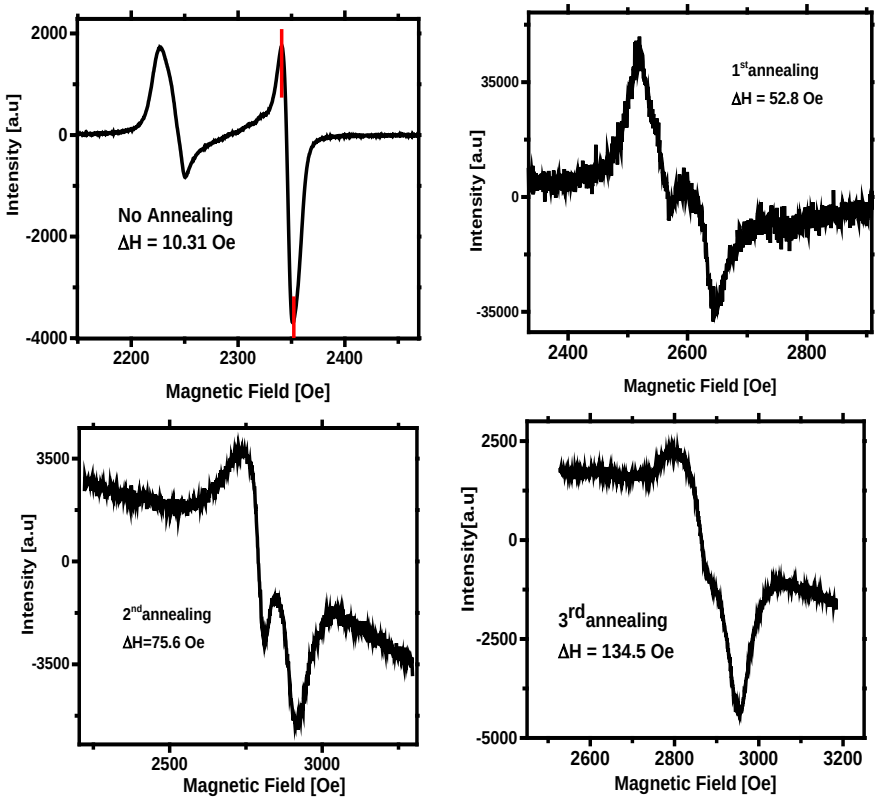


Figure 11: Annealing effect on PLD-YIG; additional annealing procedure resulted in increased line-width. The annealing was performed at approximately 800C in oxygen environment.

the line-width increase suggests oxygen deficiency due to annealing, and the line-width is found to increase to values comparable to the values of metallic ferromagnets. For example, the CoFeB has a line-width of 50 Oe, as shown in figure 12. This is not an indication that the whole film is turning metallic but rather the surface modification that is enough to cause a change in line-width. As reported and confirmed by XPS a mild Ar treatment can lead to a minor improvement and lower the line-width values which was explained the reduction or the etching process for the deficient iron at the surface.[59]

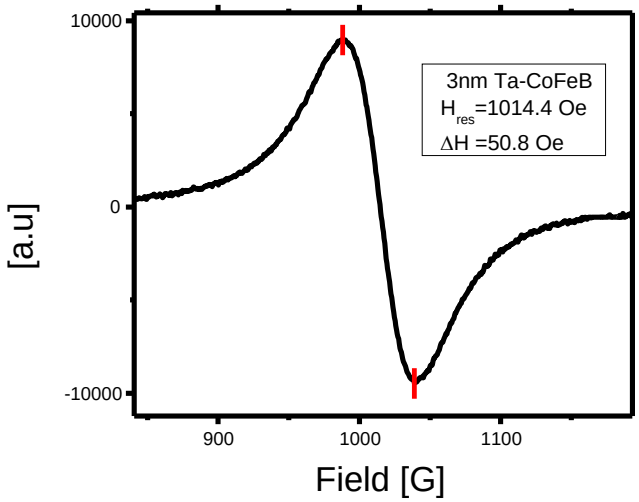


Figure 12 : FMR of CoFeB caped with Ta. Metallic ferromagnetic film exhibits usually large line-width.

We should notice the change in the number of peaks as well compared to the first FMR data in figure 7. A dramatic decrease in the number of peaks has occurred. This reduction in the number of peaks leads us to conclude that the extra peaks are not intrinsic spin wave signals. It is the degree of uniformity of the film that determine the number of

peaks. At the microscopic level, we can assume that the film would consist of two or more magnetically different parts, or regions with defects. The distribution of the defects or the magnetic parameters such as the magnetization or anisotropy in those regions of the film cause the resonance to occur either below or above the uniform resonance filed of the entire film. Due to this sensitivity, FMR spectroscopy is a powerful tool that can detect any changes in the magnetic properties of the samples. A simple test is to cut the sample to smaller size and find out if some peaks will disappear or any change on the line-width will appear figure 13 shows the change in the FMR spectra after cutting the sample from 6mmx4mm to a smaller size of 2mmx2mm. Starting with a well-defined recipe of growth, the initial sample has a small line-width (7.88 Oe) and almost a single or few Lorantzian peaks. Cutting the sample to smaller sizes results in no extra peaks and smaller line-width compared to the initial sample; and others with extra peaks and different values of line-width compared to the starting sample. In general, this practice does not cause a dramatic change; the change in line-width has been limited to 20% maximum of increase; and 5% in decreasing the line-width. This practice helps increase the yield of more PLD films by growing on large wafers. Figure 13 show the cutting effect.

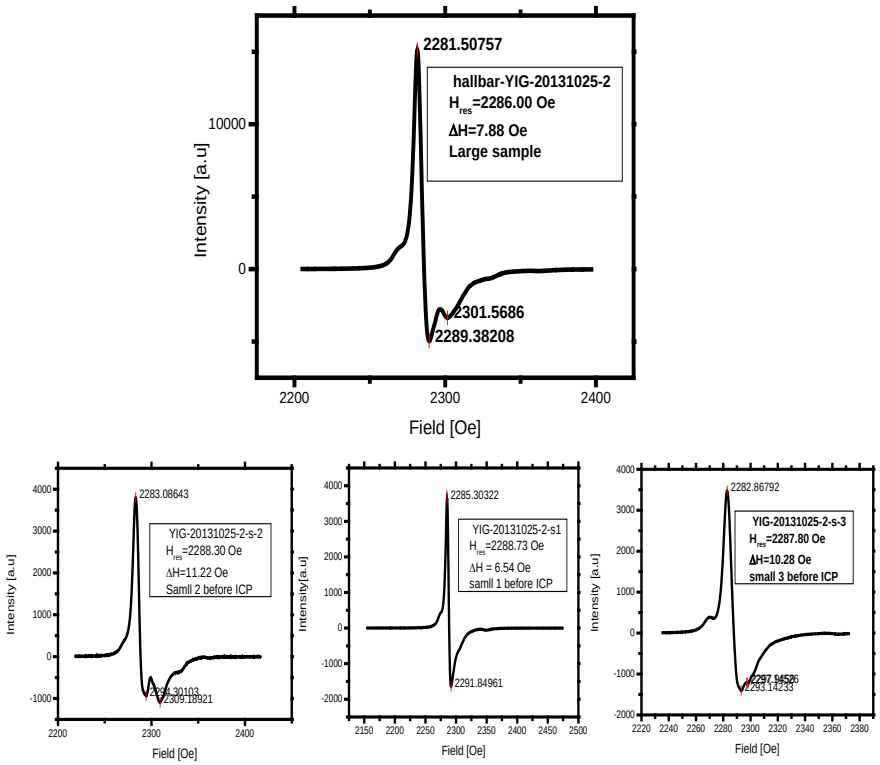


Figure 13: FMR spectra for a large YIG sample and small ones obtained by cutting the large film. At least one of the small samples has a better line shape and a smaller line-width compared to the large sample.

For possible YIG device applications, it is important to shape the structure by taking the advantage of dry etching such as Reactive Ion Etching (RIE) or Inductive coupled plasma (ICP). Both techniques are being used as standard tools in semiconductor industry and basic research. To confirm the feasibility of dry etching, the ICP method is used to etch YIG films and FMR measurements are performed after the etching. Figure 14 show the YIG FMR spectrum before and after 10 minute of ICP. This etching is performed using energetic Ar ions only without the need for any extra gases or chemical process.

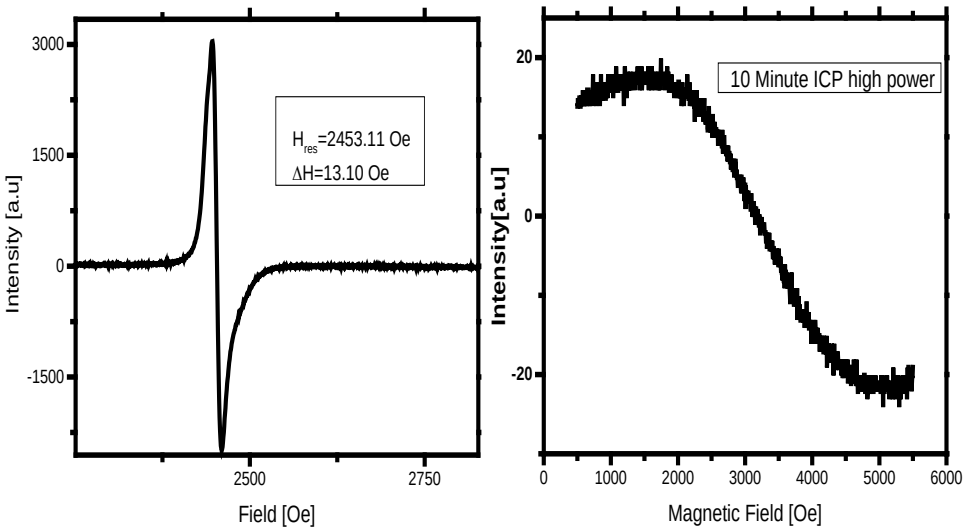


Figure 14: YIG FMR (left) before and (right) after the ICP process. One of the main advantages of nanometric thick YIG films is the ease with which they are etch using highly energized Ar particles.

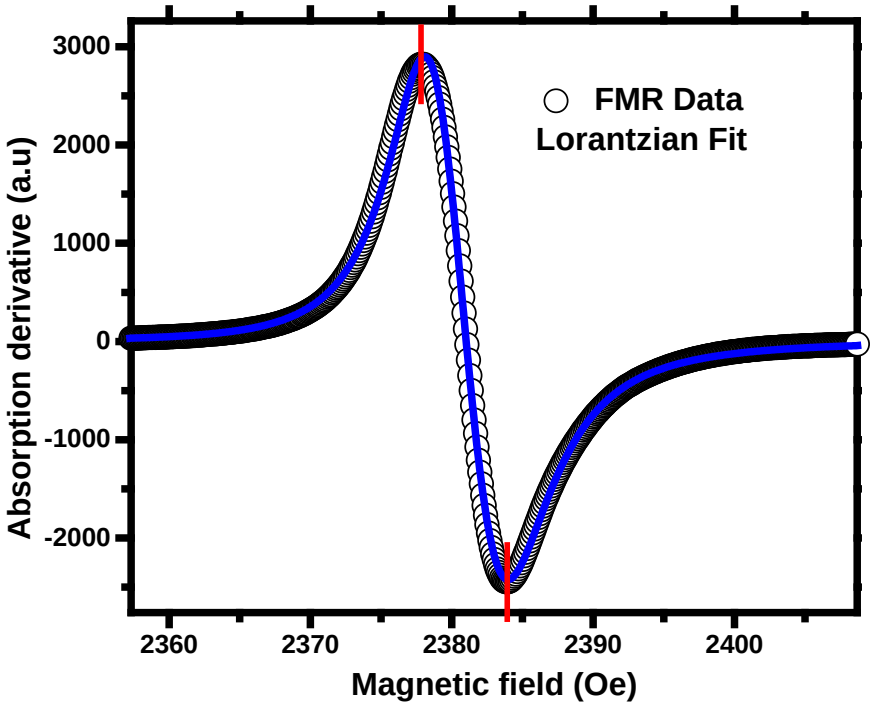


Figure 15: Single peak PLD-YIG FMR spectrum. The line is a single Lorentzian fit.

Finally we show that it is possible to obtain a more uniform YIG film that can be fitted with single Lorentzian peak. Even if the line-width is above 10 Oe, this should be expected for extremely thin ferromagnetic films. This enhancement in Gilbert damping is the topic of the next chapter. Now we will focus our attention on the possibility of obtaining high quality YIG film either from the point of uniformity or narrow line-width. Figure 15 show a uniform film obtained without any further treatment for the surface. Only by controlling the temperature of growth and the ozone pressure a magnetically uniform film can be obtained.

The narrow line-width was achieved shown in figure 16 also without the extra treatment for the film after growth. In treatment we mean chemical, mild milling, annealing, mechanical polishing and so on. This narrow line-width is among the smallest line-width that has been reported for few nanometer thick PLD-YIG films were the typical range of peak to peak width at 9.2 GHz FMR lay between 8 Oe to 20 Oe. It is smaller than that of the off-axis magnetron sputtering YIG films that have been reported by two groups recently[62, 63]. Sputtering is more suitable for a mass production of YIG films. But up to now PLD grown YIG films exhibit a flatness that cannot be achieved easily with sputtering technique, which is extremely important to carry out fundamental and application related studies.

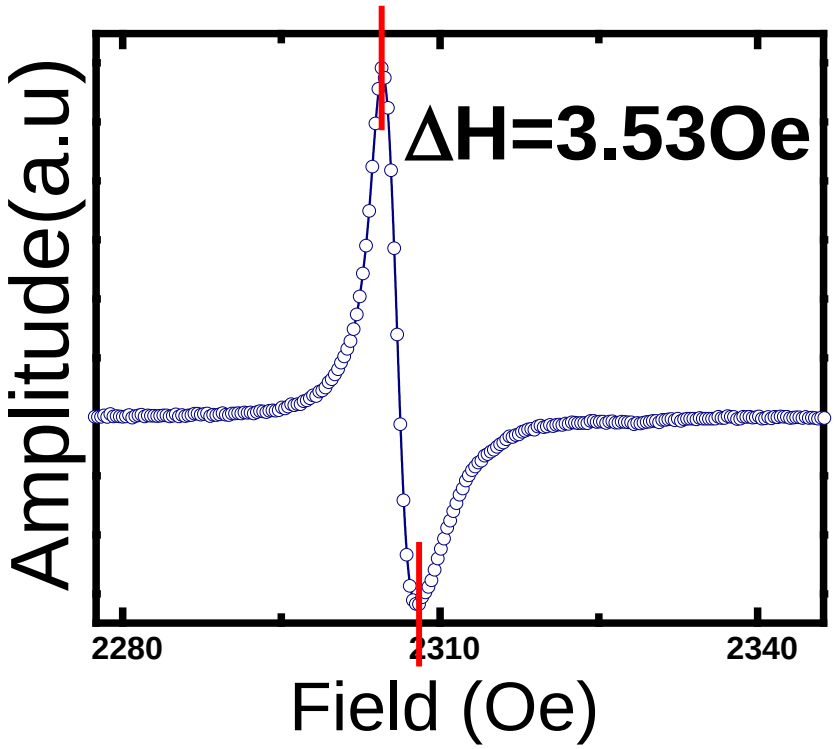


Figure 16: FMR spectrum with an extremely narrow line-width from a uniform film

## Enhancement of Gilbert damping

The second term in the Landau-Lifshitz-Gilbert (LLG) equation has been introduced by Gilbert in 1955[64]. The dimension less parameter α is called Gilbert damping constant. From figure 1 if this term is absent, or $\alpha = 0$ then the magnetization $M$ will precesses around the effective magnetic field vector with frequency $\omega = \gamma H_{eff}$. When the Gilbert damping turned on $\alpha > 0$, the precession of the magnetization will spiral toward the effective magnetic field direction. The relaxation time is inversely related to the Gilbert constant $t \propto \frac{1}{\alpha\omega}$. The microscopic damping mechanisms in ferromagnetic materials is not well understood, even though it is a subject of many theoretical[65, 66] and experimental[67] studies. In thin films, the interest is largely driven by the potential applications such as high density magnetic recording. More recently, new fundamental concepts related to damping have been explored, for example switching of the magnetization under the influence of spin-current.[68-70]

The Gilbert damping constant exhibits an enhancement when the magnetic film thickness is reduced to nanometric thickness limit. First enhancement of Gilbert constant has been observed in metallic layered system of Cu-Co and Pt-Co[69, 71]. The enhancement was by one and two orders of magnitude compare to cobalt bulk damping constant α=0.007[72].

This enhancement is also observed in ferromagnetic insulator YIG films. Figure 17 shows the FMR measurements for several YIG thicknesses and very pronounced enhancement is observed as the thickness is lowered down to 20 nm.[52]

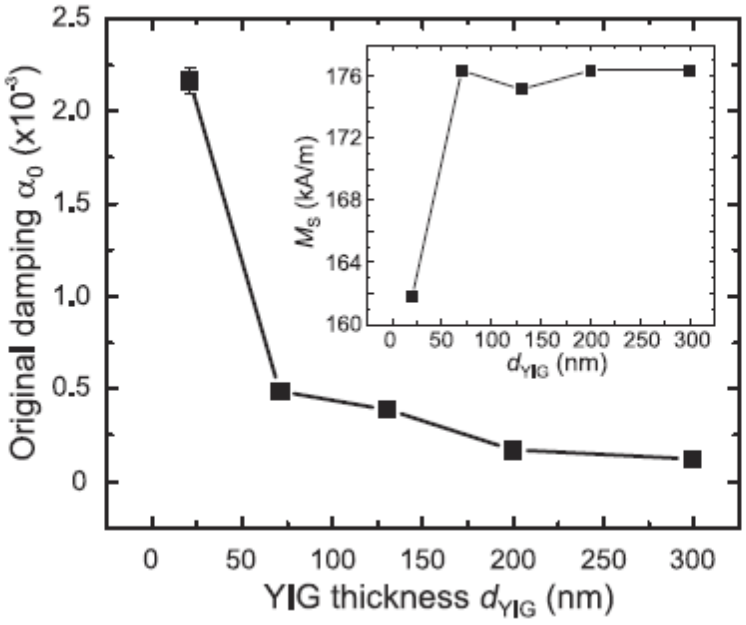


Figure 17: Damping enhancement when reducing the thickness of YIG film.

This increase in the Damping constant specially at the 20 nm thick YIG and bellow is interpreted to be driven by the electron-magnon scattering at the interface for metallic thin films, and two-magnon scattering in ferromagnetic insulators due to the increase of the ratio between surface to volume in thin films.[73]

This kind of damping enhancement realized in the magnetic materials is due to the energy redistribution within magnetic subsystem such as magnon-magnon scattering or energy redistributions to a magnetic subsystems like phonons, charge scattering. In this work we will focus on a different kind of damping that occurs when attaching a ferromagnetic film to a nonmagnetic metal. This damping leads to an extra distribution of

the energy to the nonmagnetic metal. Spin pumping can generate a spin current which can behave as a damping mechanism that has been investigated in metallic systems and recently in insulators as well.

A capping layer of high spin-orbit coupling normal metal exerts a strong effect on polarized currents in magnetic layered structure. Pt, Pd, Ta and W are of intense interest due to the large spin Hall effect, a phenomena that enable the conversion between charge and spin currents;[74] Via the invers spin Hall effect (ISHE) a DC voltage is generated from pure spin current which is pumped into high spin-orbit normal metal is used as a method to study the spin Hall effect.

Then studying the behavior of the Gilbert damping under varying thickness of the normal high spin-orbit coupling metal is necessary to utilize the spin Hall torque in measoscale spintronic based devices.

## Spin Mixing Conductance

Spin mixing conductance refers to the efficiency with which the spin current across at the NM/YIG interface are generated. For this, a Pd or Ta metal was deposited on YIG film by the mean of sputtering technique.To study the thickness effect, Pd or Ta of increasing thickness was deposited sequentially. And a careful FMR measurement was carried out for each thickness of the same material. The spin mixing conductance can be determined from the damping enhancement. This is from the well-established formalism under using single frequency FMR. The formula [75] given by

$$G_{Re}^{\uparrow\downarrow} = \frac{e^2}{h}\frac{2\sqrt{3}\,\pi\, M_s \gamma\, t_F}{g\,\mu_B \omega}\,(\Delta H_{YIG|NM} - \Delta H_{YIG})$$

$G_{Re}^{\uparrow\downarrow}$, is the real part of the spin mixing conductance, $M_s$ the saturation magnetization, $\gamma$ gyromagnetic ration, $t_F$ is the thickness of the ferromagnetic layer, $\Delta H_{YIG|NM} - \Delta H_{YIG}$ the peak to peak width for the caped film and pristine one. $G_{Re}^{\uparrow\downarrow} = 2 \text{ x } 10^{14}\Omega^{-1}m^{-2}$.

For our PLD-YIG film $G_{Re}^{\uparrow\downarrow}$ value is the highest among all the reported values literature, this might be due to the flatness of the sample. This is in agreement with the theoretically predicted values figure 18 and figure 19 is the experimental data. In addition, it provides an insight on the cause of the enhancement of the damping under varying the metal thickness. From first principles calculations an enhancement in mixing conductance value is observed upon the insertion of an metallic iron layer between the normal metal Ag and YIG this insertion leads to an increase of 40-65% in the mixing value. Our FMR experimental data figure 19 reveal the similar values but an increase in mixing value occurred without the insertion of Iron layers. This is a clear indication that the first few layers of Pd are behaving as a ferromagnetic metal. Which navigate to call the increase in the enhancement of damping α Magnetic Proximity Effect.

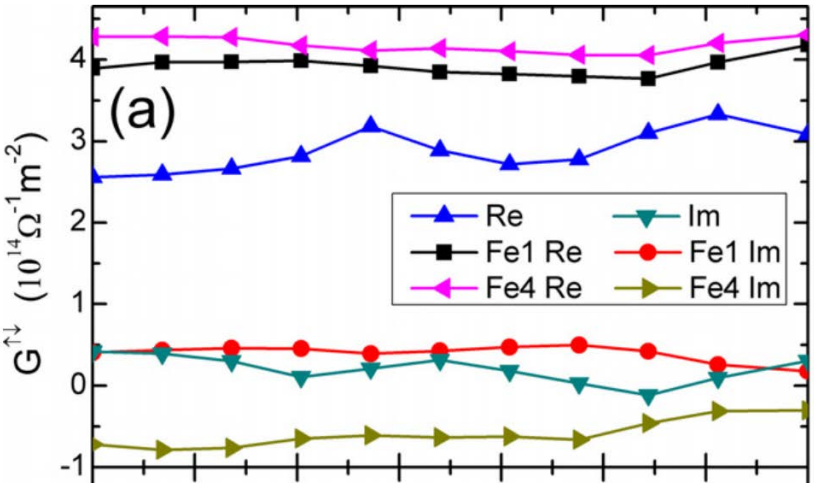


Figure 18: Real part of spin mixing conductance based on DFT. 40-60 % increases when inserting an iron layer between YIG and Ag.

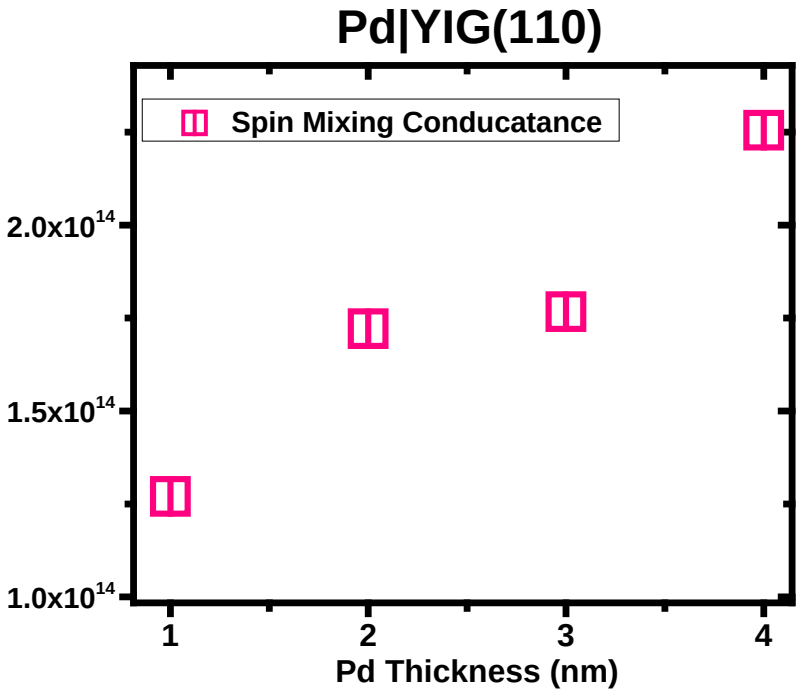


Figure 19: Spin mixing conductance obtained from FMR at 9.2 GHz. For YIG|Pd bilayer system.

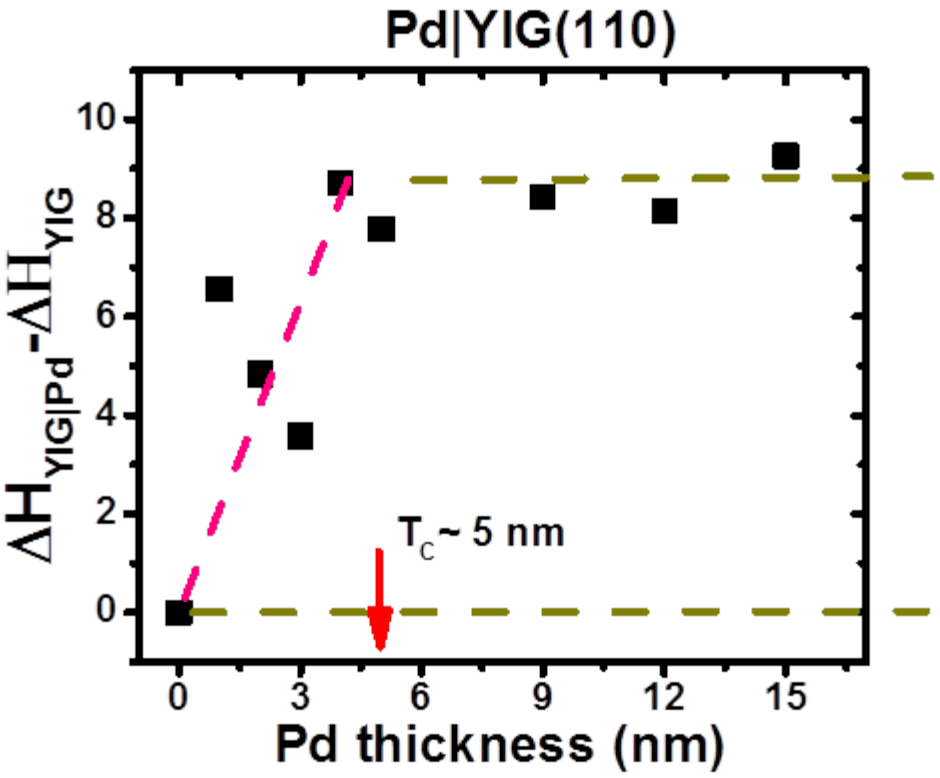


Figure 20: Enhancement of the damping upon increasing the thickness of the Pd normal metal thickness, linear increase and critical thickness of 5nm before saturation is a common features under varying the Pd thickness.

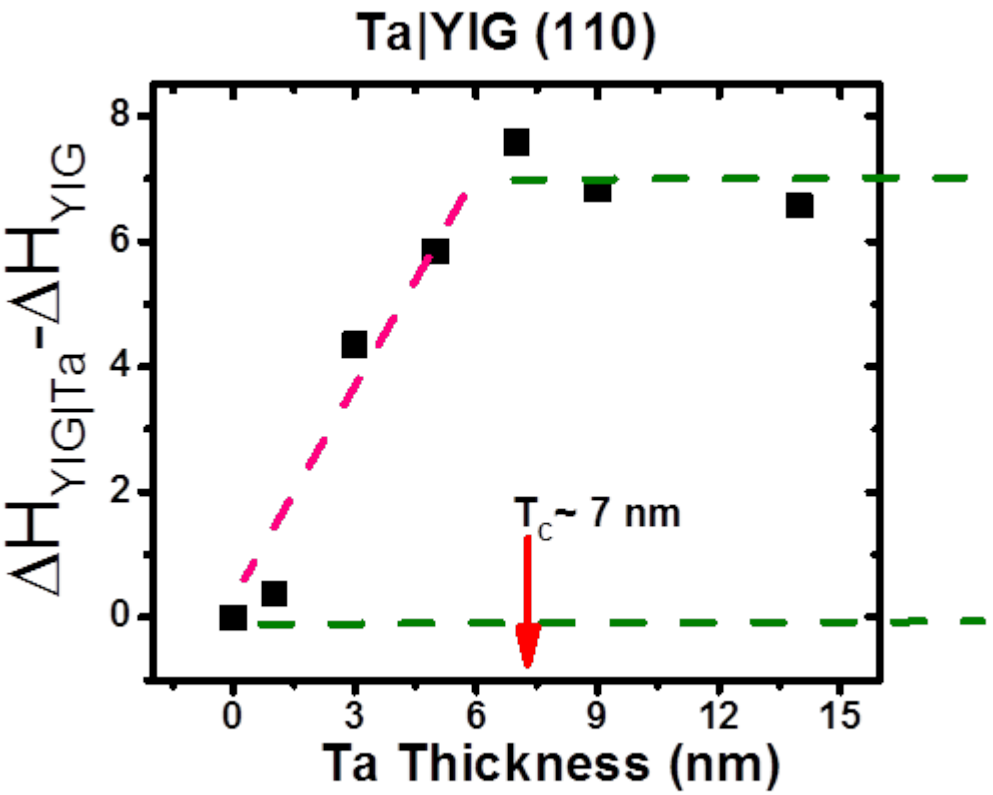


Figure 21: Enhancement of the damping upon increasing the thickness of the Ta normal metal thickness, linear increase and critical thickness of 7nm before saturation is a common features under varying the Ta thickness.

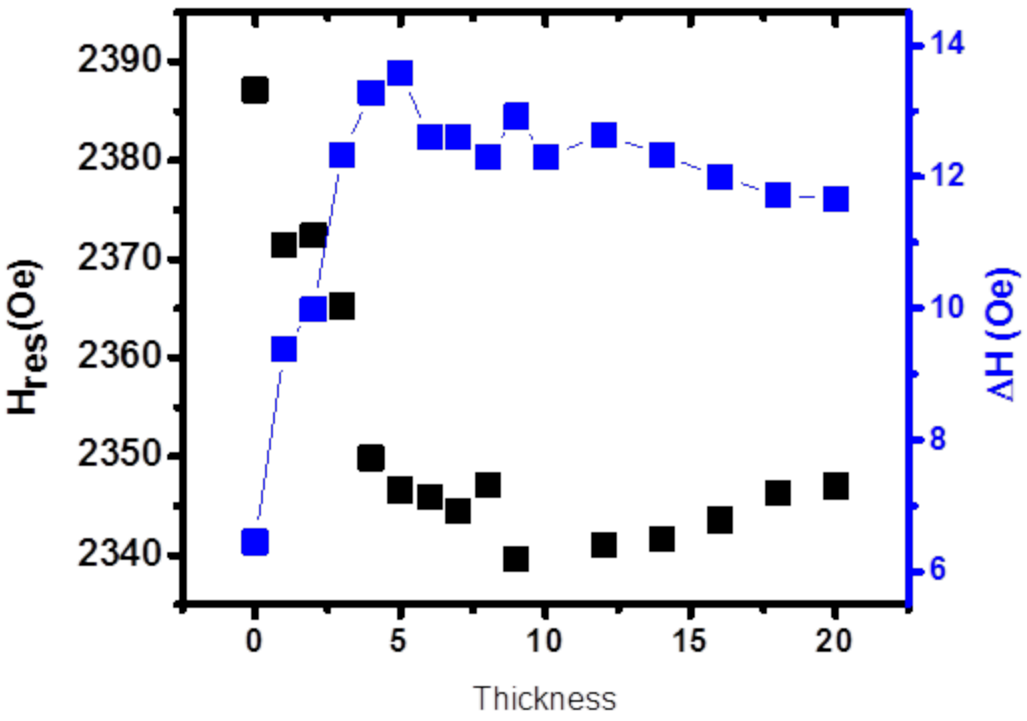


Figure 22: FMR under varying Pd from 0nm to 20 nm, the critical thickness where saturation appear are 5nm. The increases in damping is about 45% and the. The increases in damping are associated with decrease in resonance field. Both saturate at the same thickness. The change in saturation filed is related to static damping. This enhancement in damping can be explained by the existence of magnetic proximity effect at the interface.

## Damping enhancement with increasing paramagnetic layer thickness

The first report on the damping upon increasing the paramagnetic layer thickness was reported in in Pt|YIG[6] and Pt,Pd|Py [42]separately. X-ray magnetic circular dichroism

(XMCD) was carried out on the metallic bilayer systems and confirmed the proximity on both paramagnetic metal Pt and Pd.

We have carried out a direct exchange FMR under varying the paramagnetic metal Pd and Ta while keeping YIG film fixed. Figures 20, 21, and 22 show a linear increase in the damping before saturation. And the critical thickness of Pd is about 5nm and Ta is about 7nm. The increase in damping for Pd and Ta do extend ~ 80% before get saturate. The enhancement part before saturation can be fitted with linear line using:

$$\Delta H_{YIG|NM} = \frac{\Delta H_{saturation} t_{NM}}{t_c}$$

At room temperature, the spin diffusion length, which is defined as the travel distance which a non-equilibrium spin population can propagate; is evaluated to be about 9.2nm[76, 77]Ta spin diffusion length is estimated to be ~2nm[50] form Invers spin Hall measurement and 2.7 from non-local spin valve measurement[78]. These two values obtained by transport measurement which is ballistic over the spin current scattering range.

This damping is indeed an interfacial phenomena and it's possible to estimate the interfacial exchange coupling for Pd and Ta only when knowledge of the induced moment on both do exists either by XMCD or first principle. This energy could be obtained by equating the Zeeman energy with the interatomic exchange energy given by:

$$J_{ex} = \frac{1}{2} \frac{< M >}{\mu_B N_0 F} \frac{t_p}{t_i}$$

Figure 22 show the enhancement of $\Delta H$ is associated with the decrease of resonance field $H_{res}$, the enhancement of line-width do corresponds to the dynamical damping. The resonance field is a static constant and the decrease might be explained by interfacial exchange energy and the exchange energy of the ferromagnetic YIG. From the above equation the thickness average paramagnetic moment <M> will decrease as the thickness of the paramagnetic layer increase.

This experiment revealed new damping, where the energy is transferred to external system as in spin pumping. And the results showed an agreement with what has been reported for Pd on metallic system in term of the critical thickness where the saturation start. This critical thickness depends on the choice of the normal metal. In Pt it's ~2nm, Pd and Ta 5nm and 7nm respectively. At room temperature the spin diffusion length showed disagreement between the transport obtained values and FMR saturation one. We would argue that a single measurement system is needed in this case to clarify this issue. We are proposing performing spin pumping in cavity and thickness as well for the same sample to overcome this disagreement. Also spin pumping will provide an insight on the spin Hall angle as well which is very important for the estimation of the spin current density.

## Linear and nonlinear excitation

In order to distinguish if the phenomena of enhancement of line-width or resonance filed change are not due to the non linear excitation effect. Nonlinearity played an important role in solid state devices. In order to investigate the nonlinear effects we performed microwave

power dependent on single YIG thickness while varying the normal metal thickness. Power dependent experiment on different YIG film thickness has been reported recently[52]. What has been reported is the power dependency on varying the YIG layer thickness under keeping the normal metal fixed? concluded that for thin YIG film 20nm and 70nm the power dependency is linear. The non-linear effect at higher thickness were attributed to four magnon scattering.

Studying the high power effect under varying the normal metal thickness are very important from several point of view. First, the spin current depends on the spin diffusion length of the normal metal. Second, the active layer that the spin current is detected throw is the normal metal because YIG is an insulator. The third point the normal metal shows a thickness dependence that. Last, recently sputtered YIG showed an extremely high value of invers spin Hall voltage[62] at high microwave power with six order of magnitude larger than what has been reported by any group. This might only explained by the non-linear effect on spin pumping. Figure 23 shows the effect of varying power from 200nW to 200mW on YIG|Pd. The first observation that the line-width and resonance field increase simultaneously with increasing the power.

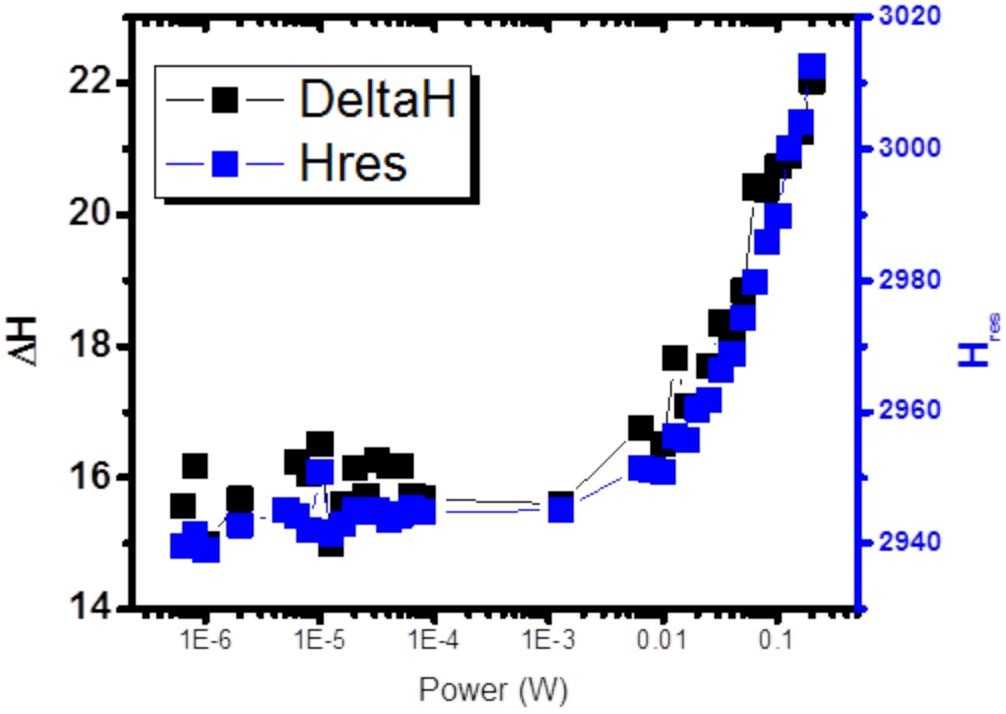


Figure 23: FMR Power dependence an increase in both line-width and resonance field occur under varying the power. This set of data reveals the linear part of power dependence to avoid fold over effect which is below 1mW.

When varying the thickness of the Pd layer the increase of the line-width and resonance field is observed in all samples. And the non-linear turning point can be extracted to be at the power value of 0.6 mW. At first, we should recall from enhancement of Gilbert damping data in previous section all are performed at the linear part with power of 20 uW. At low power we have enhancement in line-width as we increase the thickness and decrease in resonance field simultaneously. At high power, we can observe different behavior the resonance or line-width will increase for the first up to ~2 nm thick Pd then will decrease as the Pd thickness is increased.

As in figure 24 and 25 this can be explained in phenomenological way; if the spin current is generated from YIG into Pd, then this spin current will defused in based on the spin diffusion length. The only way to support this argument is the fact that at high microwave power the generated invers spin Hall signal are amplified. This means at high power it is possible to generate more pronounced spin current. As we increase the thickness of Pd this spin current will dissipate into the extra layers which will lead to reduction in the signal. Also it's possible to claim that the first few layers of Pd are not uniform or they do not form a continues Pd film. This non-uniformity with the previous knowledge that the Pd will exhibit a magnetic moment at the interface lead us to conclude the YIG surface non-uniformly corrugated. Such a surface will provide a well suitable environment for magnon-magnon scattering. As we increase the thickness of the Pd layer this scattering will be suppressed and a reduction in line-width and resonance field at high thickness will occur at high power.

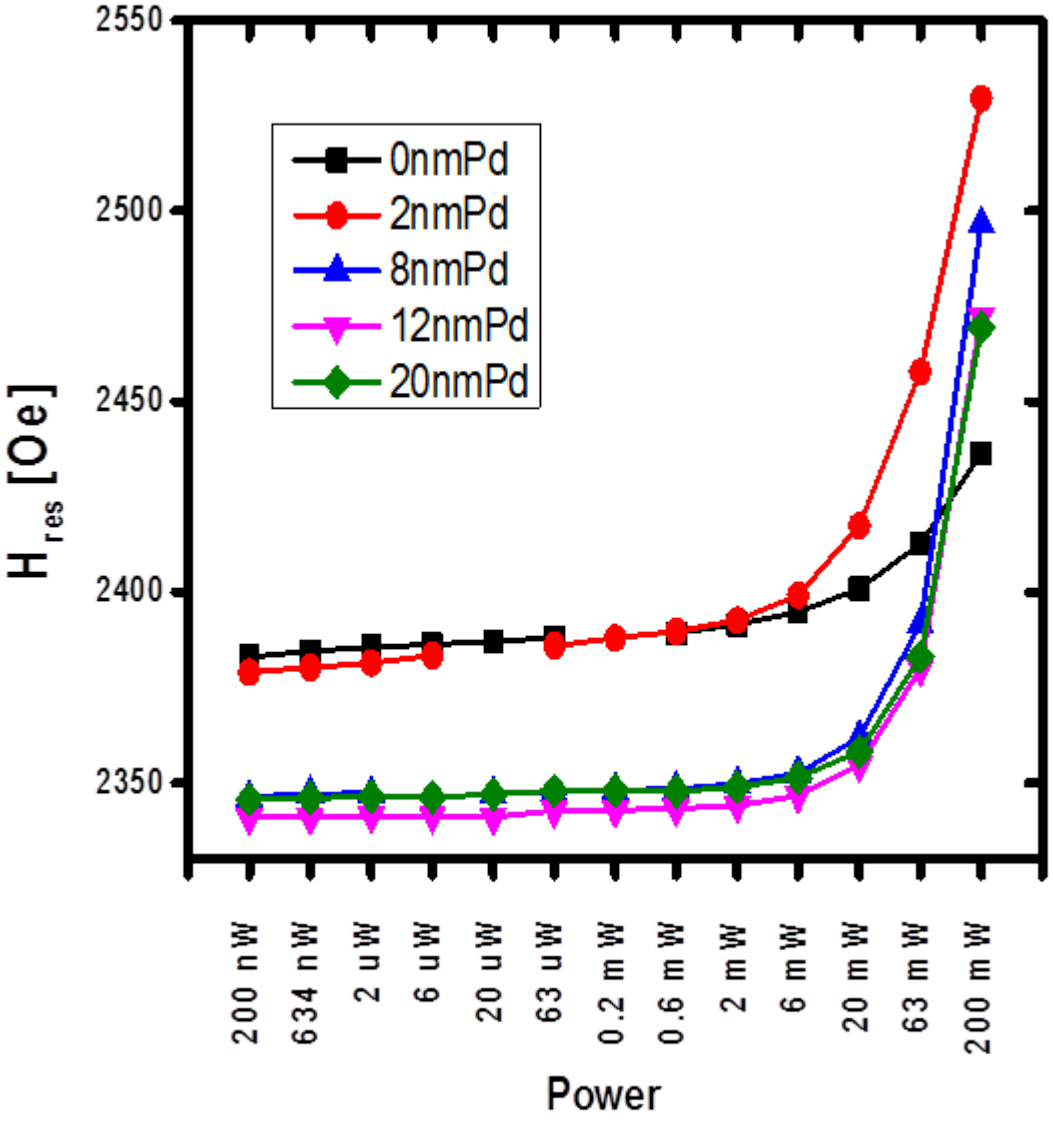


Figure 24: FMR power dependence under varying the Pd thickness on YIG. At low power, the resonance is decreasing as we increase the thickness. At high power different behavior is observed and the signal are in disagreement with the linear past the FMR resonance for less Pd is higher than the YIG film and the value start decreasing but all are above the YIG resonance filed.

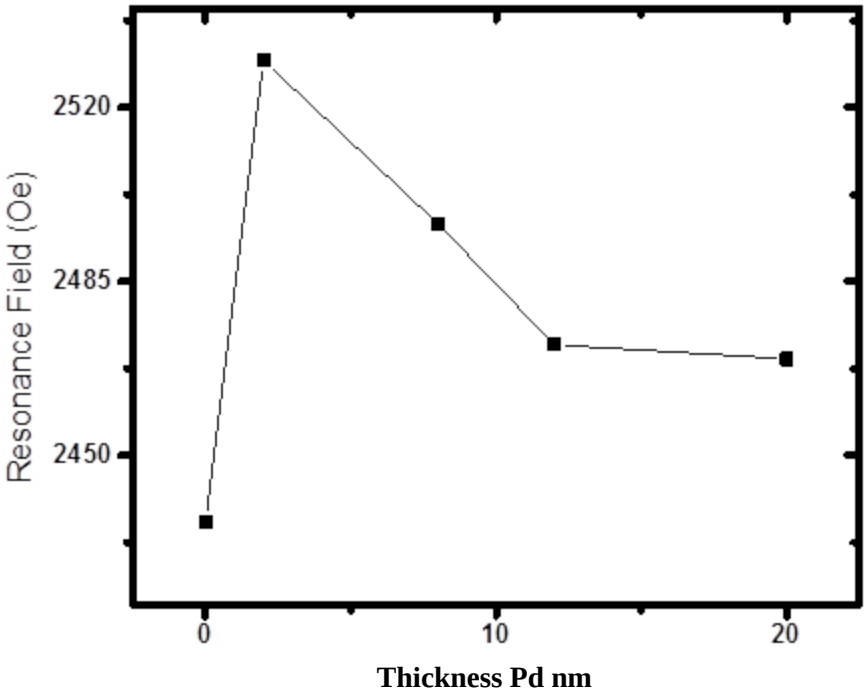


Figure 25: FMR resonance field at 200 mW power value for different thickness, the maximum thickness is at 2nm which might be considered the critical thickness or the spin diffusion length of Pd. At maximum power, the IVSH voltage exhibit higher values. The increase and decrease shape mimic the shape of spin magneto resistance vs spin diffusion length where the peak represent the spin diffusion length.

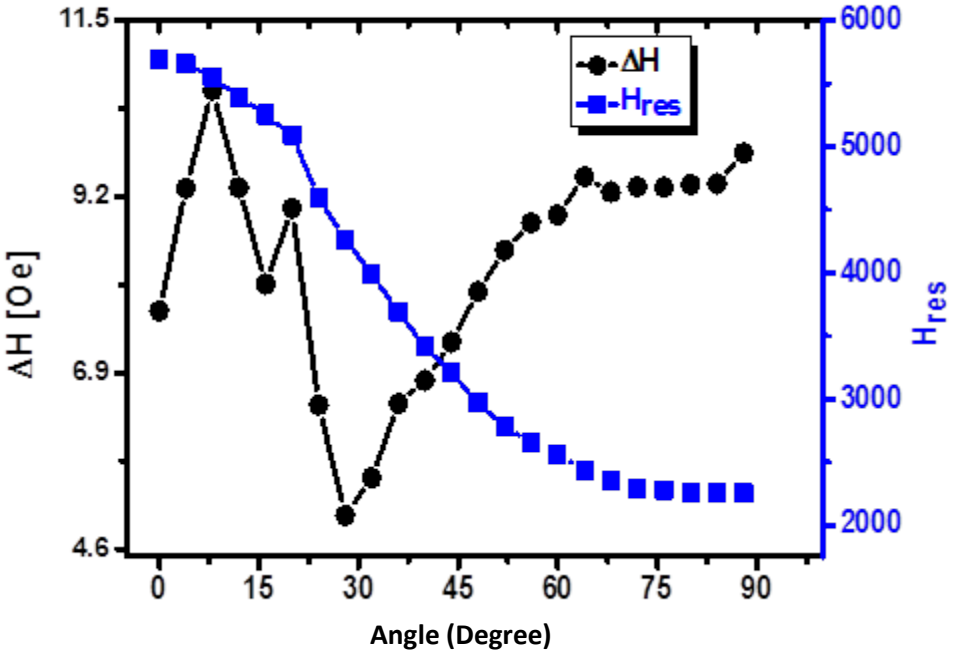


Figure 26 : FMR angular dependence, the solid square are the resonance files at different out of plan angles. The solid circles are the line width corresponded to each angle, the dependency of line width on angle indicate the existence of extrinsic damping.

## Magnon-Magnon interaction

To support the concept of magnon-magnon scattering in our YIG|NM system, an angular dependent FMR at fixed frequency were carrier out. Basically the out of plane angular dependent FMR has been used as a method to identify the intrinsic damping contribution to the line-width which is the Gilbert damping; and the extrinsic damming contribution which results from defect and sample inhomogeneity in thin magnetic film. This intrinsic and extrinsic damping can be expressed by[79]:

$$\Delta \boldsymbol{H}_{\boldsymbol{total}} = \Delta \boldsymbol{H}_{\boldsymbol{intrinsic}} + \Delta \boldsymbol{H}_{\boldsymbol{extrinsic}}$$

It’s not enough to justify the two magnon scattering from the angular dependency only. However in thin film with small inhomogenetiies the two-magnon explanation[80] is more pertinent than the local resonance model[81], and the equation of summing intrinsic as Gilbert contribution and extrinsic as two-magnon contribution can explain the inequality between the line-width representing external field inplane and line-width corresponding to line-width of field out of plan $\Delta H_{\parallel} \neq \Delta H_{\perp}$. Figure 26 represent the FMR angular dependency where we can see clearly the inequality of line-width.

## Current Induced Spin Hall Torque

The spin Hall effect (SHE) describes the conversion of longitudinal charge current $J_c$ into transverse spin current $J_s$, the origin of which in normal metal is the spin-orbit coupling. Normal metals with high spin-orbit coupling such as Pt can generate a pure spin current without being in proximity or contact with ferromagnetic material. The high spin-orbit coupling will deflect conducting electrons with different spins into opposite directions. The SHE has attracted intense interests because it generates a pure spin current

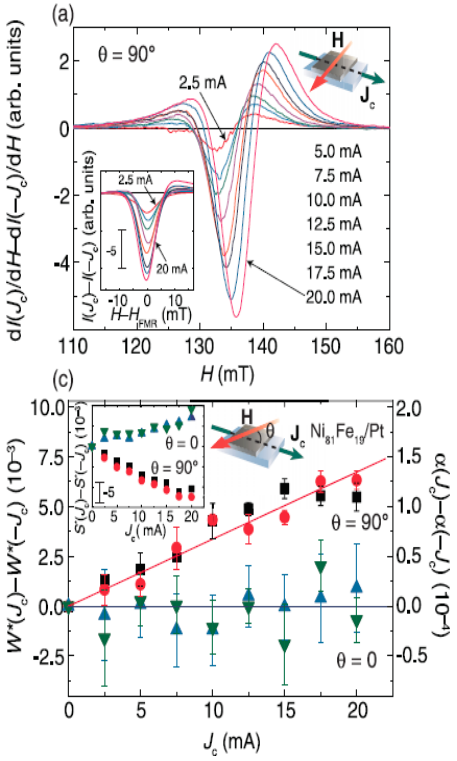


Figure 27: First Spin Hall FMR experiment on metallic system Py|Pt [7].

which might be a promising for spintronic based solid state devices. We will use this effect to induce a torque on the ferromagnetic film.

Current induced spin torque ferromagnetic resonance (ST-FMR) demonstrated very well in ferromagnetic metal and normal metal bilayers systems.[7] The effect is possibly contaminated simultaneously by the Orested field and Joule heating, but can be distinguished by the different symmetry of the resonance under applying current with opposite polarity. Figure 27 shows the first metal based ST-FMR data.

In ferromagnetic insulator YIG this phenomena has been demonstrated in micrometer thick film[5] and reproduced by another group recently on the same thickness level[3]. The first report has demonstrated a very low current density $11.1 \times 10^{8} \mathrm{Am}^{-2}$

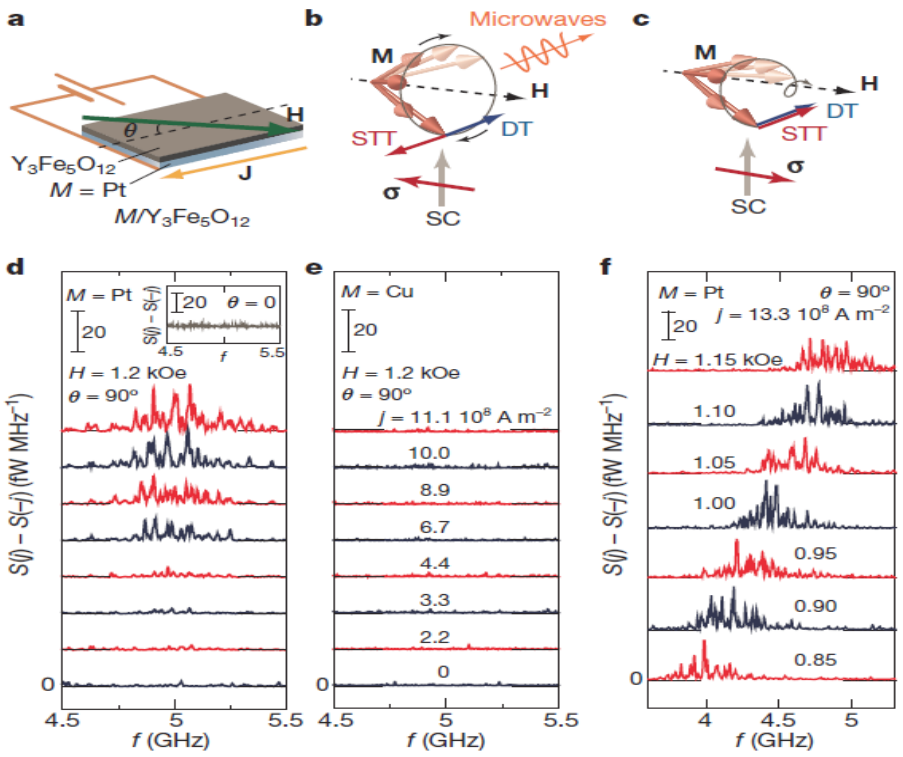


Figure 28: FMR-spin Hall torque on YIG as reported in the first observation of transmission of electrical signal in ferromagnetic insulator. [5]

needed to induce spin transfer torque compare to the theoretical prediction by two orders of magnitude Figure 28, and very high current density 2 x $10^{10}$Am$^{-2}$ by the reproduced result on thick YIG film as in Figure 29.

The first attempt to carry out this effect on 200nm thick film concluded that the ST-FMR does not exist at this very low thickness[50]. Despite this conclusion, it is worth to test the effect on PLD nanometric thick film specially after confirming the quality and high

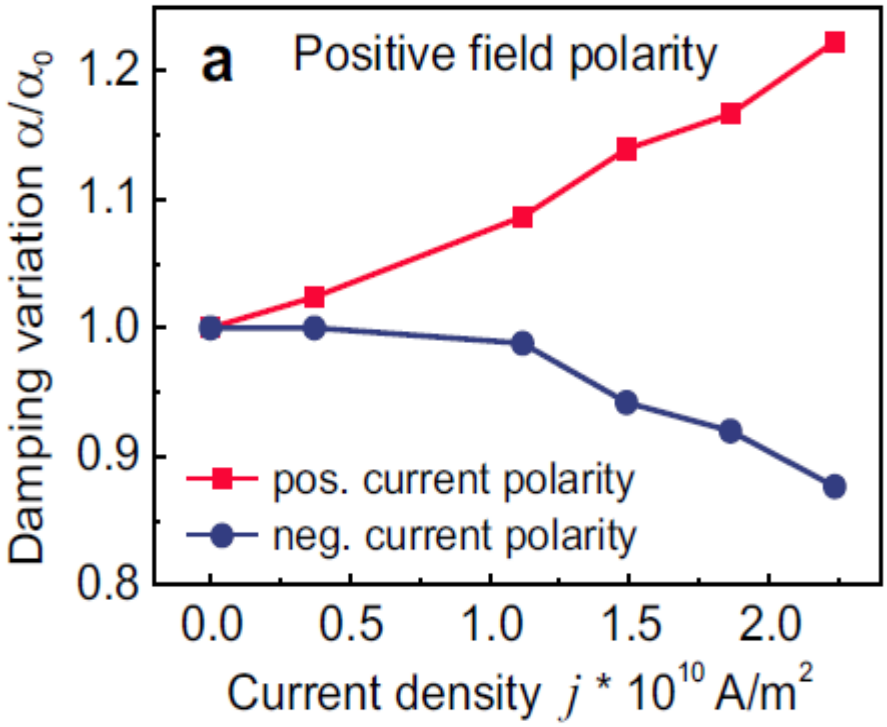


Figure 29: FMR current induced spin Hall torque on few micro thick YIG, current density are within theoretical prediction. [3]

mixing conductance factor. Alos many questions should be addressed due to the set of opportunistic effects such as Joule heating, or Oersted field.

Figure 30 shows the effect of current in 20 nm thick Pd film on ~ 30 nm thick YIG film. The first advantage that we have a single peak FMR spectrum, then at any current, we can distinguish easily any if the FMR signal introduce any noisy and chaotic signal.

Second, to remove Joule heating, we can subtract the opposite current polarities similar to what has been done for metallic bilayer systems.

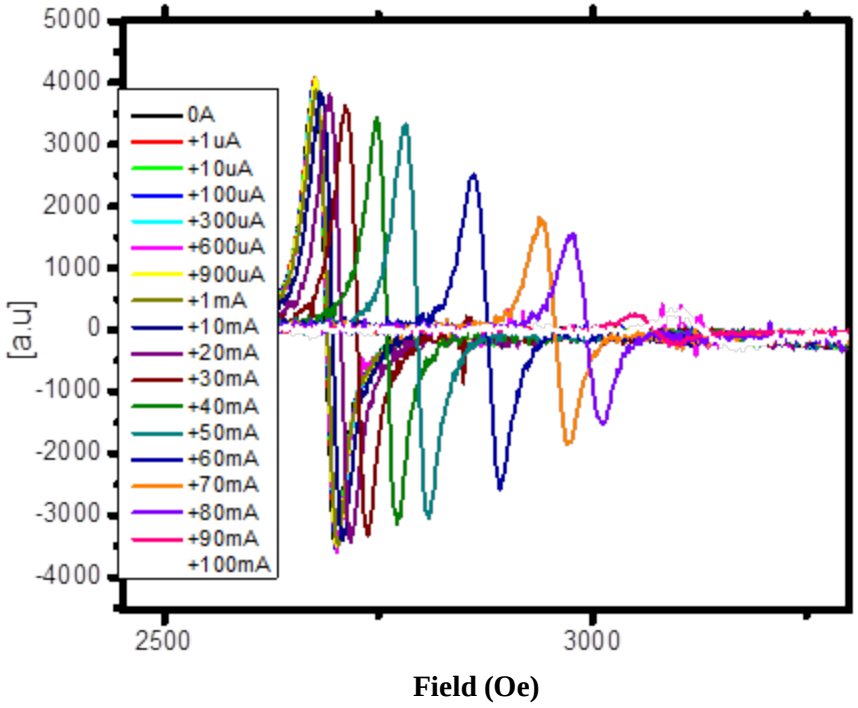


Figure 30: current applied perpendicular to the DC filed, from 1uA to 100mA. A clear change occur on the FMR signal. Shift in the resonance field, decrease in intensity, increase in line width. Total signal contains heating effect, Orested field effect, and spin Hall effect.

From figure 30 we can notice a very clear current effect on the FMR spectra when applying a current perpendicular to the DC field. The more noticeable effect is the decrease in intensity of the spectrum as the current is increased, and more important is the shift in the resonance field. These two observations will help us test the heating effect and identify the heating contribution to the FMR signal. When heating takes place, the sample temperature

will rise. This process is not instantaneous. We have indeed observed a time dependent relaxation in the ST-FMR. After we apply a current to the metal film, the FMR spectrum evolves with time, and gradually settles over a period of time. This settling time depends on the magnitude of the current for a fixed sample. In practice, this time dependence was not reported before but is expected and should be avoided by waiting a sufficiently long time. Then the first important thing is to determine the relaxation time. Figure 31 shows that to relax the FMR completely at 15 mA it took about 1 hour, then to collect a signal of positive and negative 15 mA we need to spend 4 hours at least before collecting FMR spectra of another current value. From the time dependent resonance field curve we can devide the spectrum into two part: the initial linear increase and approaching saturation. This linear part is re-plotted in figure 32.

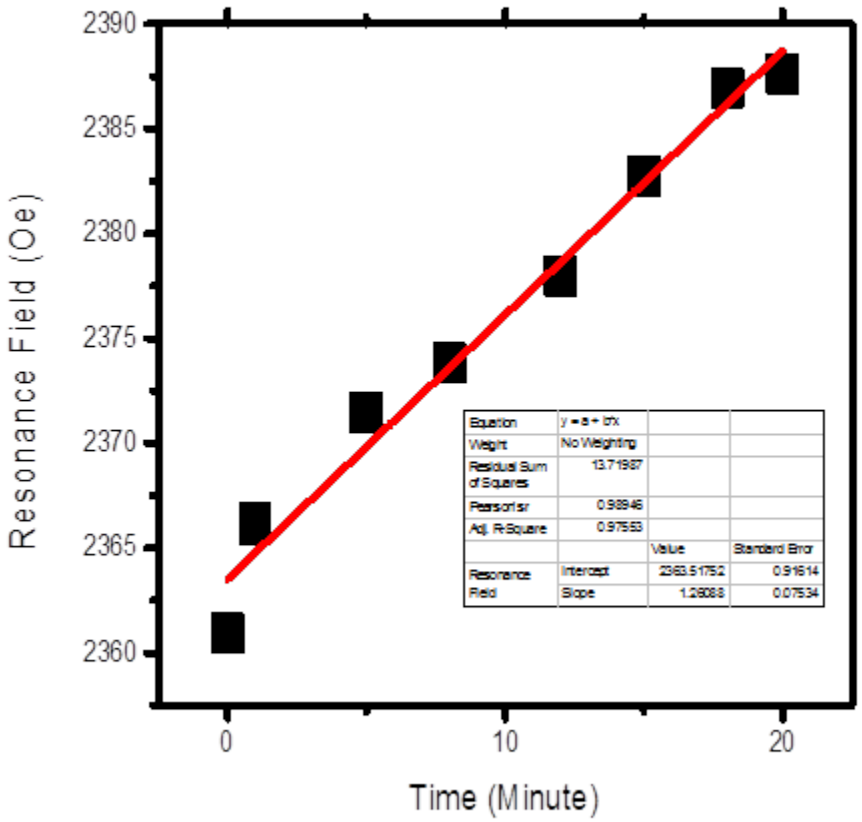


Figure 31: The linear part before saturation of the resonance field vs. time at 15mA.

the slope of the linear part we can see that the resonance field shifts about 1.2 Oe per minute to reach the turning point before saturation. The best way to understand the origin of this relaxation process is to carry temperature dependent FMR on the bilayer system without applying current and observe the temperature dependence of the resonance filed.

Figure 33 show the experimental data of FMR spectrum under varying the temperature from 100 K to room temperature.

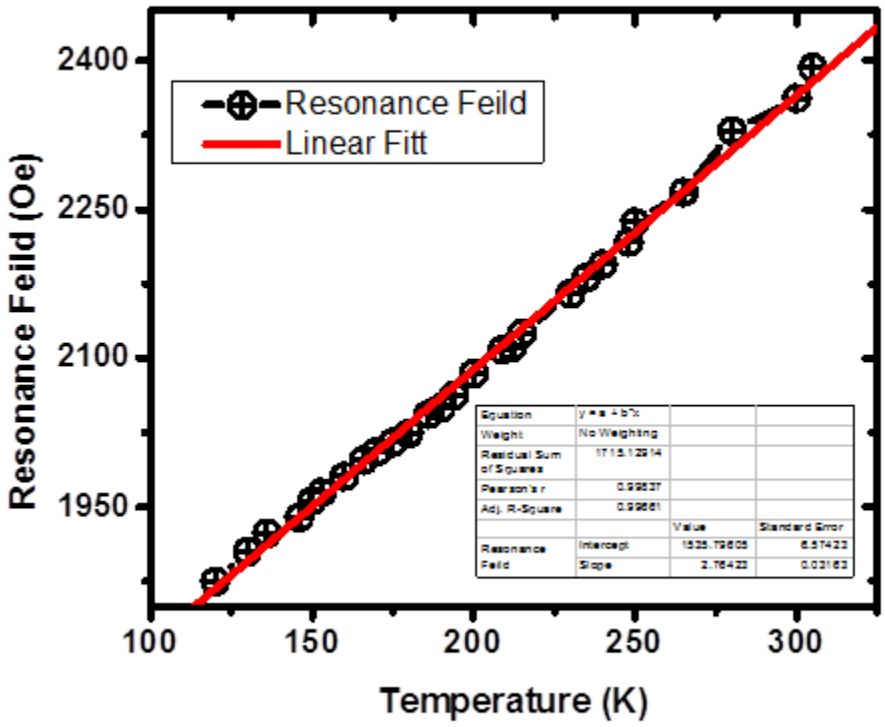


Figure 32: Resonance field vs. temperature data. The solid line is the linear fit.

The resonance filed behaves linearly in temperature and with a change of 2.1 Oe/K. From the current effect data we can see that the change of about 30 Oe in the linear part at least took place. From the temperature dependence data we can find out how much temperature gradient is needed to induced a change of 30 Oe on the resonance field. It turns out it requires about 11 K to induce a change of 30 Oe on the resonance field. 11 K is a possible value of the-temperature rise to be produced from a current in the metallic film. Then it is possible to propose using FMR as a thermometer to estimate the effect of heating produced from the current in this type of experiment. Then temperature dependence and shift in FMR

spectrum is resolved and the best way to exclude the heating effect from the spectrum is by making sure that the resonance filed of positive current and negative current do reach the complete saturation so that the temperature variations is out of the picture.

The second point we should take into account is the Oersted field effect when applying a positive or negative current on the sample based on Ampere's law this current will generate a magnetic field. The subtraction of the FMR spectra of different current polarities will remove this effect. Based on Ampere law it’s possible to estimate the absolute value of this field and VSM measurements can estimate the magnitude of the effect as well. This field is less than 10 Oe. Figure 34 shows VSM data and the current effect as well which we can clearly observe it at the high filed side. From the inset we can demonstrate the Orested filed effect which is about 10 Oe, and it is consistent with Ampere law.

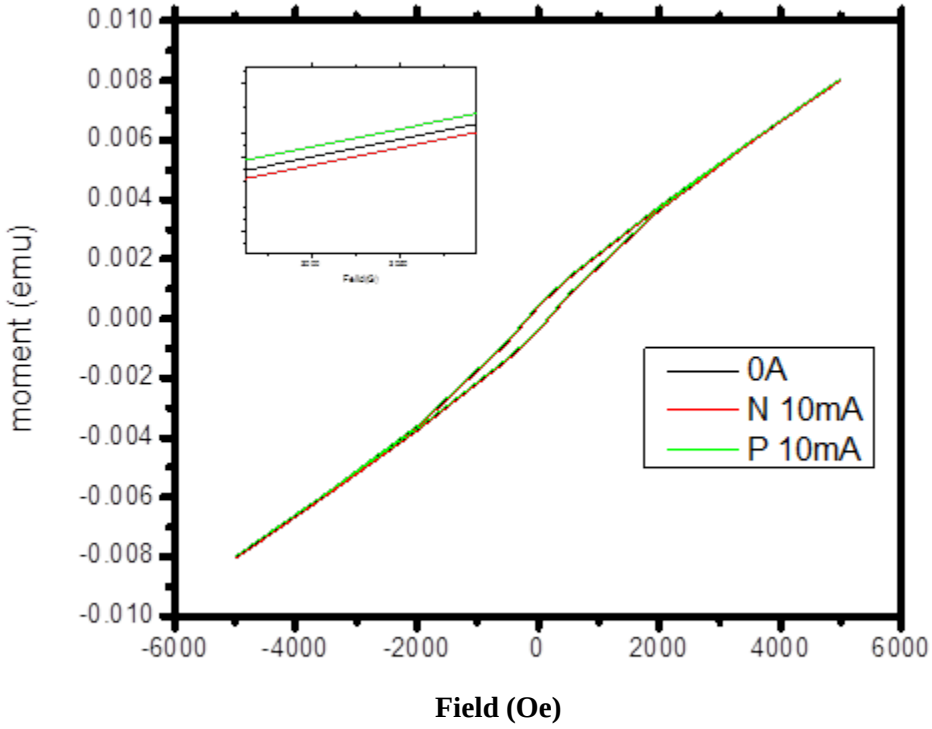


Figure 33: VSM measurement for the same sample with 10 mA current applied to the sample to find out the Oersted field contribution.

Now it is ready to analyze the effect of current to see if any torque contribution due to the fact that Joule heating and Oersted field can be excluded after subtracting the stable FMR of different current polarities after a long wait time. The noticeable change in line-width at least can be observed without carrying any subtraction at 1mA. Due to time limitation in

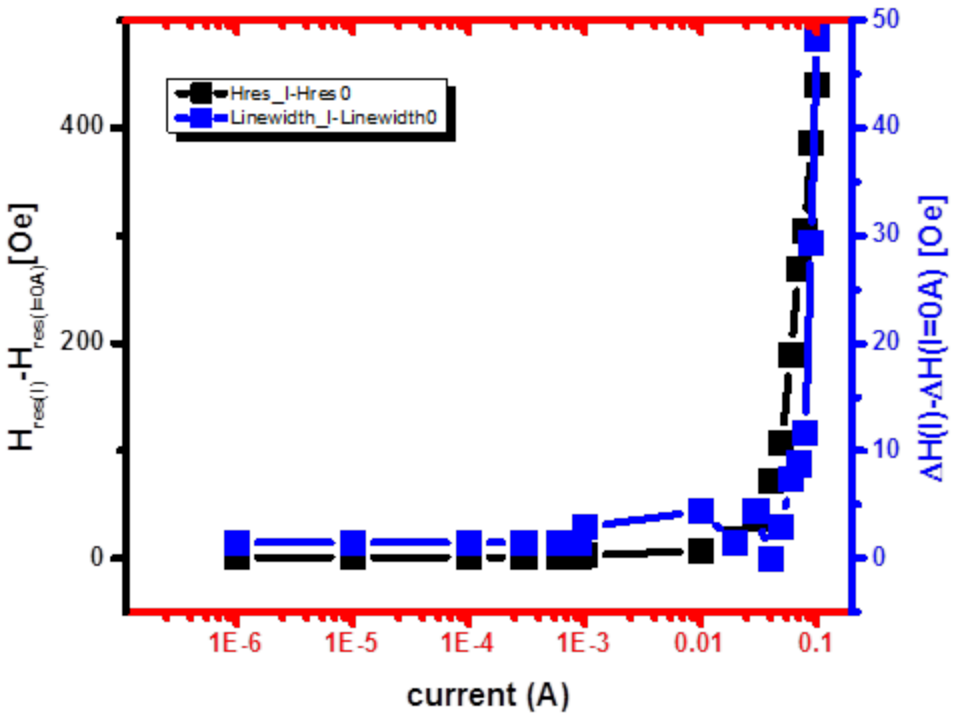


Figure 34: DC current effect on the resonance field and line-width clear change in line-width appears at 1mA.

achieving the complete saturation in the FMR spectra for mA current range, we will limit ourselfes to current values in the range of 1mA to 10 mA at first since the heating effect is small. Figure 35 shows the point at which the applied current takes pronounced effects on line-width.

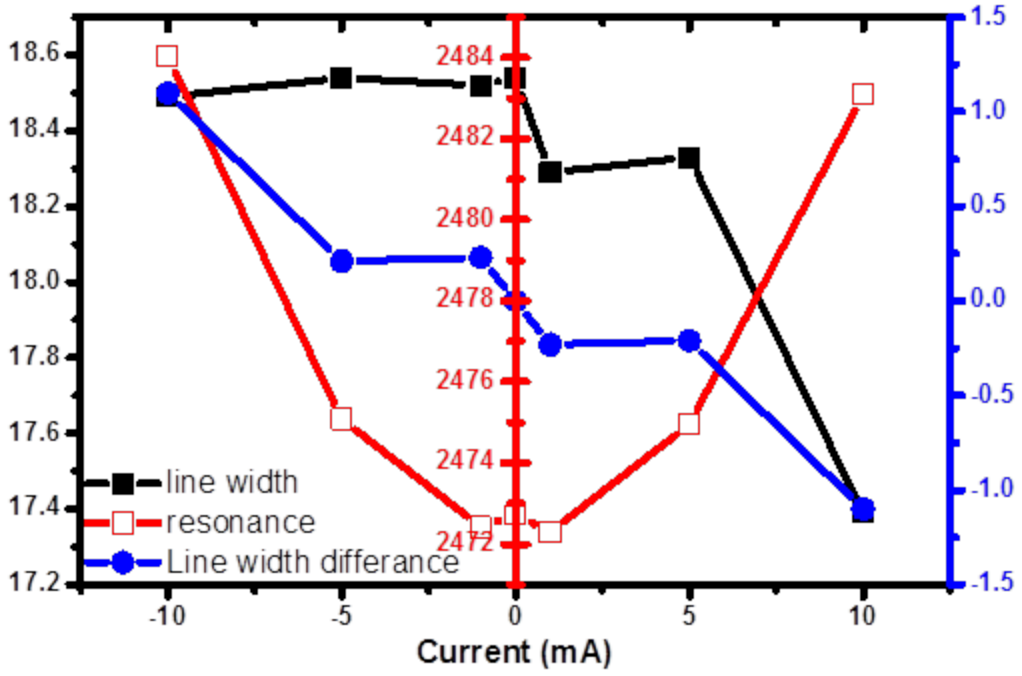


Figure 35: Solid circle represent damping and anti-damping effect. The solid square represent the line-width change at different DC current values. The square data represent the resonance field at each current.

Figure 36 shows a set of data represent resonance field, line-width, and subtracted line-width. The data collected when the system at each point is fully relaxed. Resonance filed demonstrated almost symmetric shape which is expected if the change on resonance filed is due to heating. A tiny change in resonance field can be overwhelmed by developing or engineering this experiment by providing an efficient heat sink under the YIG film. This might be possible by growing YIG on a normal metal instead of GGG substrate, the normal metal should exhibit a low spin orbit coupling to avoid the ST-FMR effect. The final structure of the system will be a tri-layer system of YIG film sandwiched between tow metals; this structure will eliminate the heating effect.

The line-width can clearly indicate that positive current is playing the role of anti-damping and the negative current is enhancing the damping of YIG film. from figure 36 one can identify the magnetization precession direction with respect to the effective field direction. But most importantly is identifying the current density to exert spin Hall torque on YIG film. For our film at 1mA has exhibited an extremely low current density to exert torque on YIG film with a value of $J_c \sim 12 \times 10^6 \frac{A}{m^2}$ this value compared to the previously

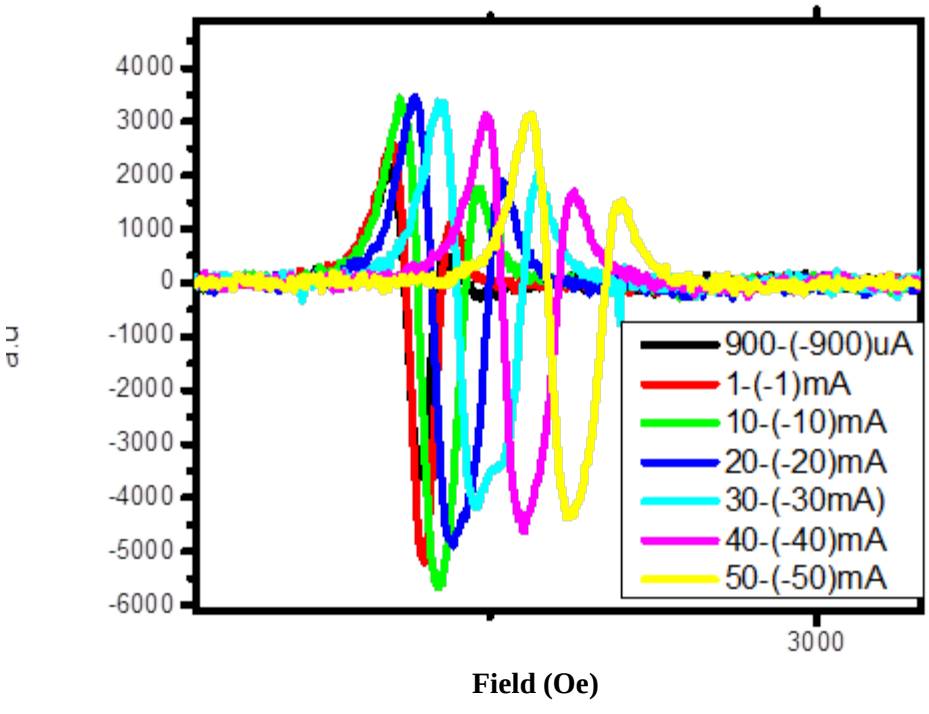


Figure 36: FMR modulation after subtracting positive and negative current to exclude heating and Oersted field effect.

reported results is two orders of magnitude less than what has been reported by the first group, and four orders of magnitude less than what is reported by the second one Figure 28 and 29 respectively.

We take advantage of the single peak YIG film then a subtraction of the signals for two current orientations: one perpendicular to the applied DC field and the second one parallel to the applied DC field. From the first one we expect a modulation in the FMR spectrum and from the second one we expect the absence of the effect due to the fact that the current is inducing any effect of damping and anti-damping on the line-width of the film. Figure 37 show similar behavior to what has been reported for Pt|Py film and clearly demonstrates the effect of spin Hall torque on the YIG film as well. Figure 38 shows when current is parallel with DC field no modulation is can be observed which fit the expectation and agree very well with the concept of spin Hall effect.

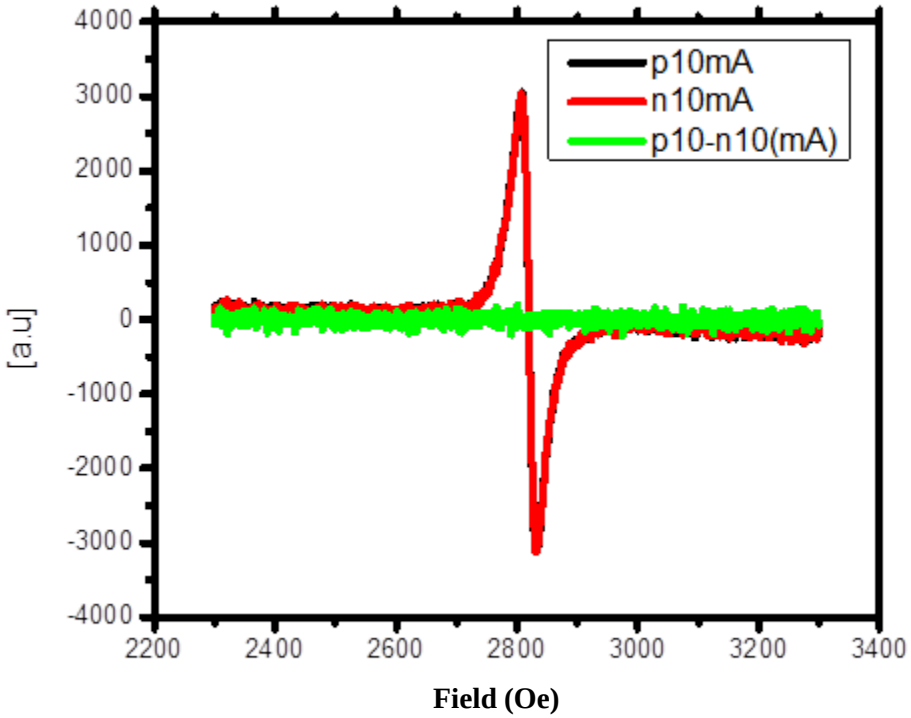


Figure 37: When the DC current is parallel to the DC field no modulation in FMR do occur, this is a clear evidence that spin Hall effect is what cause the modulation in FMR.

# Conclusion

Ferromagnetic resonance experiment for bilayer system consisted of ferromagnetic insulator and normal metal (FM|NM) revealed new ferromagnetic damping attributed to the magnetic proximity effect. This conclusion based on the enhancement in spin mixing conductance. The magnitude of this new damping depends on the thickness and the type of the metal. A critical thickness where the enhancement in line-width in Pd or Ta is larger than the spin diffusion length. At high a microwave power 200mW, this critical thickness is comparable to the spin diffusion length in Pd.

Under applying DC current on this bilayer system, the disentanglement of Oersted field effect, Joule heating effect, and spin Hall torque (SHT) effect was possible due to the uniformity of the nonmetric thick YIG film. The uniformity verified by FMR spectrum, which can be fitted by a single Lorentzian. The Oersted field experimentally estimated by VSM. The Joule heating contribution verified by temperature dependent FMR. And the spin Hall torque FMR from the damping and anti-damping of line-width also from the modulation in FMR spectra after subtracting the signals of the same current but opposite polarity. The transfer of angular momentum due to (SHT) from the normal metal to the ferromagnetic layer revealed the existence of spin transfer torque for a very low current density $J_c \sim 10^6 \frac{A}{m^2}$. This low value has a promising technological potential.

# References


1. Z. Qiu, K. Ando, K. Uchida, Y. Kajiwara, R. Takahashi, H. Nakayama, T. An, Y. Fujikawa and E. Saitoh, Applied Physics Letters **103** (9), - (2013).

2. apos, O. Allivy Kelly, A. Anane, R. Bernard, J. Ben Youssef, C. Hahn, A. H. Molpeceres, C. Carrétéro, E. Jacquet, C. Deranlot, P. Bortolotti, R. Lebourgeois, J.-C. Mage, G. de Loubens, O. Klein, V. Cros and A. Fert, Applied Physics Letters **103** (8), - (2013).

3. A. Chumak, M. Jungˇeisch, A. Serga and B. Hillebrands.

4. C. Sandweg, Y. Kajiwara, K. Ando, E. Saitoh and B. Hillebrands, Applied Physics Letters **97** (25), 252504 (2010).

5. Y. Kajiwara, K. Harii, S. Takahashi, J. Ohe, K. Uchida, M. Mizuguchi, H. Umezawa, H. Kawai, K. Ando and K. Takanashi, Nature **464** (7286), 262-266 (2010).

6. Y. Sun, H. Chang, M. Kabatek, Y.-Y. Song, Z. Wang, M. Jantz, W. Schneider, M. Wu, E. Montoya and B. Kardasz, Physical Review Letters **111** (10), 106601 (2013).

7. K. Ando, S. Takahashi, K. Harii, K. Sasage, J. Ieda, S. Maekawa and E. Saitoh, Physical Review Letters **101** (3), 036601 (2008).

8. M. N. Baibich, J. Broto, A. Fert, F. N. Van Dau, F. Petroff, P. Etienne, G. Creuzet, A. Friederich and J. Chazelas, Physical Review Letters **61** (21), 2472 (1988).

9. J. Bass and W. P. Pratt Jr, Journal of Physics: Condensed Matter **19** (18), 183201 (2007).

10. G. E. Bauer, E. Saitoh and B. J. van Wees, Nature materials **11** (5), 391-399 (2012).

11. J. C. Slonczewski, Physical Review B **82** (5), 054403 (2010).

12. S. Maekawa, *Concepts in spin electronics*. (Oxford University Press Oxford, UK, 2006).

13. T. Valet and A. Fert, Physical Review B **48** (10), 7099 (1993).

14. S. Takahashi and S. Maekawa, Journal of the Physical Society of Japan **77** (3) (2008).

15. C. Kittel and P. McEuen, *Introduction to solid state physics*. (Wiley New York, 1986).

16. S. O. Demokritov, B. Hillebrands and A. N. Slavin, Physics Reports **348** (6), 441-489 (2001).

17. S. O. Demokritov and A. N. Slavin, in *Topics in applied physics,* (Springer,, Berlin ; New York, 2013), pp. 1 online resource (xix, 262 pages).

18. N. Ashcroft and N. Mermin, Cited on, 26.

19. T. Schneider, A. Serga, B. Leven, B. Hillebrands, R. Stamps and M. Kostylev, Applied Physics Letters **92** (2), 022505 (2008).

20. K. Uchida, J. Xiao, H. Adachi, J. Ohe, S. Takahashi, J. Ieda, T. Ota, Y. Kajiwara, H. Umezawa and H. Kawai, Nature materials **9** (11), 894-897 (2010).

21. M. D'yakonov and V. Perel, Soviet Journal of Experimental and Theoretical Physics **33**, 1053 (1971).

22. J. Hirsch, Physical Review Letters **83** (9), 1834 (1999).

23. S. O. Valenzuela and M. Tinkham, Nature **442** (7099), 176-179 (2006).

24. T. Kimura, Y. Otani, T. Sato, S. Takahashi and S. Maekawa, Physical review letters **98** (15), 156601 (2007).

25. E. Saitoh, M. Ueda, H. Miyajima and G. Tatara, Applied physics letters **88** (18), 182509 (2006).

26. H. Nakayama, M. Althammer, Y.-T. Chen, K. Uchida, Y. Kajiwara, D. Kikuchi, T. Ohtani, S. Geprägs, M. Opel and S. Takahashi, Physical Review Letters **110** (20), 206601 (2013).

27. Y. Lu, Y. Choi, C. Ortega, X. Cheng, J. Cai, S. Huang, L. Sun and C. Chien, Physical Review Letters **110** (14), 147207 (2013).

28. S. Geprägs, S. Meyer, S. Altmannshofer, M. Opel, F. Wilhelm, A. Rogalev, R. Gross and S. T. Goennenwein, Applied Physics Letters **101** (26), 262407 (2012).

29. S. T. Goennenwein, M. Schneider, F. Wilhelm, K. Ollefs, A. Rogalev, M. Opel and R. Gross, arXiv preprint arXiv:1307.4869 (2013).

30. X. Jia, K. Liu, K. Xia and G. E. Bauer, EPL (Europhysics Letters) **96** (1), 17005 (2011).

31. Y. Tserkovnyak, A. Brataas and G. E. Bauer, Physical Review Letters **88** (11), 117601 (2002).

32. B. Heinrich, Y. Tserkovnyak, G. Woltersdorf, A. Brataas, R. Urban and G. E. Bauer, Physical review letters **90** (18), 187601 (2003).

33. J. C. Rojas-Sánchez, N. Reyren, P. Laczkowski, W. Savero, J. P. Attané, C. Deranlot, M. Jamet, J. M. George, L. Vila and H. Jaffrès, Physical Review Letters **112** (10), 106602 (2014).

34. J. A. C. Bland, B. Heinrich and J. A. C. Bland, *Ultrathin magnetic structures*. (Springer, 2005).

35. R. Urban, G. Woltersdorf and B. Heinrich, Physical review letters **87** (21), 217204 (2001).

36. S. Mizukami, Y. Ando and T. Miyazaki, Physical Review B **66** (10), 104413 (2002).

37. C. W. Sandweg, Y. Kajiwara, A. V. Chumak, A. A. Serga, V. I. Vasyuchka, M. B. Jungfleisch, E. Saitoh and B. Hillebrands, Physical review letters **106** (21), 216601 (2011).

38. B. Heinrich, C. Burrowes, E. Montoya, B. Kardasz, E. Girt, Y.-Y. Song, Y. Sun and M. Wu, Physical review letters **107** (6), 066604 (2011).

39. H. Kurebayashi, O. Dzyapko, V. E. Demidov, D. Fang, A. Ferguson and S. O. Demokritov, Nature materials **10** (9), 660-664 (2011).

40. L. Vilela-Leao, C. Salvador, A. Azevedo and S. Rezende, Applied Physics Letters **99** (10), 102505 (2011).

41. V. Castel, N. Vlietstra, J. Ben Youssef and B. J. van Wees, Applied Physics Letters **101** (13), 132414-132414-132414 (2012).

42. A. Ghosh, S. Auffret, U. Ebels, F. Wilhelm, A. Rogalev and W. Bailey, arXiv preprint arXiv:1308.0450 (2013).

43. K. Ando, S. Takahashi, J. Ieda, Y. Kajiwara, H. Nakayama, T. Yoshino, K. Harii, Y. Fujikawa, M. Matsuo and S. Maekawa, Journal of Applied Physics **109** (10), 103913 (2011).

44. V. E. Demidov, S. Urazhdin, E. Edwards, M. Stiles, R. McMichael and S. Demokritov, Physical review letters **107** (10), 107204 (2011).

45. V. E. Demidov, S. Urazhdin, H. Ulrichs, V. Tiberkevich, A. Slavin, D. Baither, G. Schmitz and S. O. Demokritov, Nature materials **11** (12), 1028-1031 (2012).

46. L. Liu, C.-F. Pai, D. Ralph and R. Buhrman, Physical review letters **109** (18), 186602 (2012).

47. Z. Wang, Y. Sun, M. Wu, V. Tiberkevich and A. Slavin, Physical review letters **107** (14), 146602 (2011).

48. E. Padron-Hernandez, A. Azevedo and S. Rezende, Applied Physics Letters **99** (19), 192511 (2011).

49. J. Xiao and G. E. W. Bauer, Physical Review Letters **108** (21), 217204 (2012).

50. C. Hahn, G. De Loubens, O. Klein, M. Viret, V. V. Naletov and J. B. Youssef, Physical Review B **87** (17), 174417 (2013).

51. T. Chiba, G. E. Bauer and S. Takahashi, arXiv preprint arXiv:1404.2360 (2014).

52. M. Jungfleisch, A. Chumak, A. Kehlberger, V. Lauer, D. Kim, M. Onbasli, C. Ross, M. Kläui and B. Hillebrands, arXiv preprint arXiv:1308.3787 (2013).

53. J. P. Castera, Journal of Applied Physics **55** (6), 2506-2511 (1984).

54. J. E. Mee, J. L. Archer, R. H. Meade and T. N. Hamilton, Applied Physics Letters **10** (10), 289-291 (1967).

55. V. Castel, N. Vlietstra, B. J. van Wees and J. B. Youssef, Physical Review B **86** (13), 134419 (2012).

56. T. Lin, C. Tang and J. Shi, Applied Physics Letters **103** (13), - (2013).

57. T. Lin, (University of California, Riverside,, Riverside, California, 2013), pp. 1 online resource (134 pages).

58. X. Liu, Ph.D., University of California, Riverside, 2012.

59. Y. Sun, Y.-Y. Song, H. Chang, M. Kabatek, M. Jantz, W. Schneider, M. Wu, H. Schultheiss and A. Hoffmann, Applied Physics Letters **101** (15), - (2012).

60. M. J. Pechan, M. B. Salamon and I. K. Schuller, Journal of Applied Physics **59** (9), 3302-3302 (1986).

61. S. A. Manuilov, S. I. Khartsev and A. M. Grishin, Journal of Applied Physics **106** (12), - (2009).

62. H. L. Wang, C. H. Du, Y. Pu, R. Adur, P. C. Hammel and F. Y. Yang, Physical Review B **88** (10), 100406 (2013).

63. T. Liu, H. Chang, V. Vlaminck, Y. Sun, M. Kabatek, A. Hoffmann, L. Deng and M. Wu, Journal of Applied Physics **115** (17), - (2014).

64. T. Gilbert, Phys. Rev. **100**, 1243 (1955).

65. V. Korenman and R. E. Prange, Physical Review B **6** (7), 2769-2777 (1972).

66. V. L. Safonov and H. N. Bertram, Physical Review B **61** (22), R14893 (2000).

67. S. M. Bhagat and P. Lubitz, Physical Review B **10** (1), 179-185 (1974).

68. J. C. Slonczewski, Journal of Magnetism and Magnetic Materials **159** (1), L1-L7 (1996).

69. E. Myers, D. Ralph, J. Katine, R. Louie and R. Buhrman, Science **285** (5429), 867-870 (1999).

70. J. Katine, F. Albert, R. Buhrman, E. Myers and D. Ralph, Physical Review Letters **84** (14), 3149 (2000).

71. C. H. Back, R. Allenspach, W. Weber, S. S. P. Parkin, D. Weller, E. L. Garwin and H. C. Siegmann, Science **285** (5429), 864-867 (1999).

72. F. Schreiber, J. Pflaum, Z. Frait, T. Mühge and J. Pelzl, Solid State Communications **93** (12), 965-968 (1995).

73. M. Sparks, *Ferromagnetic-relaxation theory*. (McGraw-Hill New York, 1964).

74. L. Liu, T. Moriyama, D. C. Ralph and R. A. Buhrman, Physical Review Letters **106** (3), 036601 (2011).

75. E. Shikoh, K. Ando, K. Kubo, E. Saitoh, T. Shinjo and M. Shiraishi, Physical Review Letters **110** (12), 127201 (2013).

76. J. Foros, G. Woltersdorf, B. Heinrich and A. Brataas, Journal of Applied Physics **97** (10), - (2005).

77. H. Kurt, R. Loloee, K. Eid, W. P. Pratt and J. Bass, Applied Physics Letters **81** (25), 4787-4789 (2002).

78. M. Morota, Y. Niimi, K. Ohnishi, D. H. Wei, T. Tanaka, H. Kontani, T. Kimura and Y. Otani, Physical Review B **83** (17), 174405 (2011).

79. J. Dubowik, K. Załęski, H. Głowiński and I. Gościańska, Physical Review B **84** (18), 184438 (2011).

80. R. D. McMichael, D. J. Twisselmann and A. Kunz, Physical Review Letters **90** (22), 227601 (2003).

81. R. D. McMichael and P. Krivosik, Magnetics, IEEE Transactions on **40** (1), 2-11 (2004).